Journal of Directed Energy, **3**, Spring 2009, 149–191

Recent Advances in Explosive Pulsed Power

L. L. Altgilbers*
U.S. Army Space and Missile Defense Command/Army Forces Strategic Command, Huntsville, Alabama 35807

A. H. Stults
U.S. Army Aviation and Missile Research, Development, and Engineering Center, Huntsville, Alabama 35801

M. Kristiansen, A. Neuber, J. Dickens, A. Young, T. Holt, and M. Elsayed
Texas Tech University, Lubbock, Texas 79409-3102

R. Curry and K. O'Connor
University of Missouri, 349 EBW, Columbia, Missouri 65211

J. Baird and S. Shkuratov
Loki, Inc., Rolla, Missouri 65401

B. Freeman
KTECH Corporation, Albuquerque, New Mexico 87123

D. Hemmert
HEM Technologies, Lubbock, Texas 79409

F. Rose, Z. Shotts, and Z. Roberts
Radiance Technologies, Huntsville, Alabama 35806

W. Hackenberger and E. Alberta
TRS Technologies, State College, Pennslyvania 16801

and

M. Rader and A. Dougherty
Naval Research Laboratory, 4555 Overlook Avenue, Washington, D.C. 20375

Received October 7, 2008; revision received February 13, 2009.
*Corresponding author; e-mail: larry.altgilbers@smdc.army.mil.

Explosive pulsed power (EPP) has been investigated since the early 1950s. However, in the late 1980s interest in it began to decline. Interest was revived in 1998, when the Air Force Office of Scientific Research established Multidisciplinary University Research Initiative and New World Vista programs at Texas Tech University (TTU) to study explosive pulsed power devices, with an emphasis on compact or small systems. In 2004, a series of Small Business Innovative Research programs were initiated to further develop compact explosive pulsed power. On the basis of these efforts, we now have a better understanding of the basic physics of small EPP systems and of their weaknesses and strengths. As a result, we can now build reliable generators that provide consistent results and that can be utilized in practical applications. In this paper, a brief introduction to these generators will be given, along with some of the most recent advances in our understanding of them. This paper will report only on advances made by Army and Navy researchers and those of their contractors. A description of an explosive-driven high-power microwave test bed that was built at TTU will be presented. Finally, the results of recent experiments in which EPP was used to drive an antenna will be presented.

KEYWORDS: Explosive pulsed power, HPM test bed, Power conditioning, Seed sources

1. Introduction

Traditional power supplies cannot meet the volume and mass constraints imposed by many current, as well as future, platforms. To meet these imposing requirements, an enabling technology is required. It was realized in the 1950s that one way to achieve these goals was to use explosive pulsed power (EPP). Over the years, a number of EPP devices have been developed, built, and tested, and as our understanding of them improved so did our understanding of how to use them in practical applications. In recent years, there have been significant improvements in EPP, primarily due to the development of new materials and consistently funded experimental programs. Therefore, these explosive-driven systems are now being considered for a number of new applications including directed energy, powering special test equipment at remote test sites, rapid charging of capacitors, mine detection, propulsion, lightning and electromagnetic (EMP) simulators, electromagnetic launchers, mineral and oil exploration, and blasting operations at mines and quarries.

There are five general classes of EPP generators:

- magnetic flux compression generators (FCGs)
- ferroelectric generators (FEGs)
- ferromagnetic generators (FMGs)
- moving magnet generators (MMGs)
- explosive-driven magnetohydrodynamic generators (EMHDs)

Of these, only three will be discussed in detail due to their utility in several practical applications.[2] They are the magnetic FCG; the FEG, which is a high voltage source; and the FMG, which is either a high-voltage or a high-current source, depending on how it is built. Of these three classes of power supplies, the FCG is a high-energy source, whereas the other two are relatively low-energy sources. A hybrid type of generator, the shock wave generator (SWG), is currently under investigation and will be discussed because of some of its potentially unique parameters.

2. What Is Explosive Pulsed Power?

As noted earlier, the utilization of explosives to generate electrical power has been researched since the early 1950s. This concept evolved out of the nuclear weapon programs in the United States, the United Kingdom, and the Soviet Union. These countries were looking for methods to solve several technical problems including driving fusion reactions without using a fission primer, detonator arrays, and neutron sources.

EPP devices fall into one of two broad categories:

- Devices that convert the chemical energy of explosives into electrical energy by driving a conducting medium through a magnetic or an electric field. This is accomplished by transforming the chemical energy of the high explosives into the kinetic energy of a moving conducting material. This moving conducting boundary does work against the magnetic field and amplifies the electrical energy supplied by a seed source. We will call these generators *field interaction* generators.
- Devices that use the shock waves generated by high explosives to induce a phase change in a material that stores energy in the form of electric or magnetic fields. We will call these generators *phase transition* generators.

3. Classes of EPP

As noted earlier, there are five major classes of EPP generators, only three of which will be described in this paper. A hybrid class, the SWG, will also be briefly described, because it is a relatively new type of generator based on the FCG.

- FCGs (Fig. 1) use the chemical energy from *high* explosives to accelerate a metallic conductor, called the *armature,* which traps and compresses a magnetic field initially created by a seed energy source such as a capacitor bank, battery, or another EPP generator. The accelerating armature compresses the seed magnetic field trapped within a conducting shell that is composed of the armature, a stationary conductor, called the *stator*, and end *glide planes*. When the armature makes electrical contact with the input glide plane, the initial magnetic flux from the seed source is trapped, and the seed

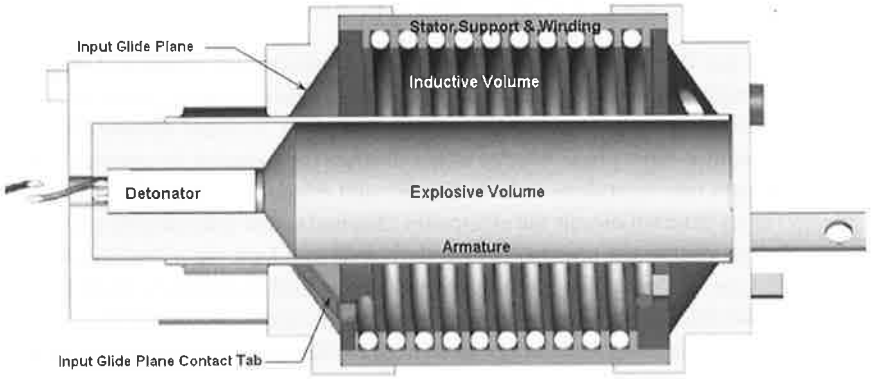

Fig. 1. Schematic diagram of a FCG. It delivers a typical energy density that is on the order of a few joules per cubic centimeter.[1]

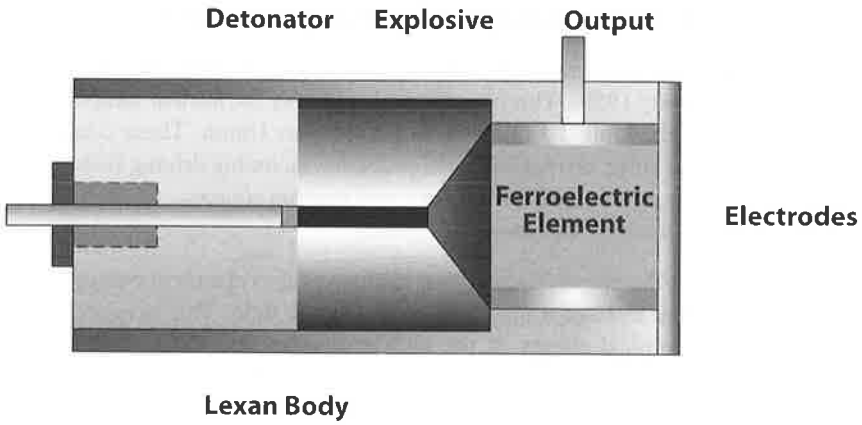

Fig. 2. Schematic diagram of a miniature transverse FEG.[3]

circuit is disconnected from the generator. This process is called *crowbarring*. When the armature makes contact with the stator, a moving electrically conducting *contact point* is established, which closes the armature–stator circuit. If the FCG is a helical generator, the contact point propagates along the wire of the helical coil (stator) as the expanding conically shaped armature propagates along the axis of the generator. Compression of the trapped magnetic flux multiplies the initial seed current flowing in the stator. This amplified current is then delivered to a load either directly or through a power conditioning circuit. The energy density of an FCG, i.e., the ratio of the electrical energy delivered to the load and the FCG volume, is typically a few joules per cubic centimeter. Note, however, that this number is dependent on the generator design and the load itself. In general, the smaller the load inductance, the higher the energy output. However, a narrow-band microwave source acts more like a resistive than an inductive load. Hence, power conditioning is typically needed, which often employs an energy storage inductor serving as the inductive load for the FCG. Note that although the FCG performs more efficiently with a small inductive load, the overall system efficiency is also determined by the power conditioning, which tends to perform better with larger inductive loads. Thus, part of designing an explosive-driven system will be the optimization of the FCG load's inductance.

- FEGs (Fig. 2) use the chemical energy from high explosives to generate a shock wave. Ferroelectric materials store electrical energy when they are externally poled by an electric field. When a shock wave passes through the poled material, it causes a phase change in the crystalline structure. This phase change either depoles the material or causes the material to transition from one crystalline state to another and releases the stored electrical charge (or energy) to an external circuit via electrodes attached to the ferroelectric element. This released electric charge (or energy) is then delivered to a load via a power-conditioning circuit. This type of generator can be used to deliver high voltages to high-impedance loads and is suitable for the direct drive of radiating circuits.
- FMGs (Fig. 3) use the chemical energy from high explosives to generate a shock wave to demagnetize a permanent magnet. Ferromagnetic materials store energy in the form of a magnetic field when they are externally magnetized. When a shock wave passes through the ferromagnetic material, it destroys the magnet and the magnetic domains within

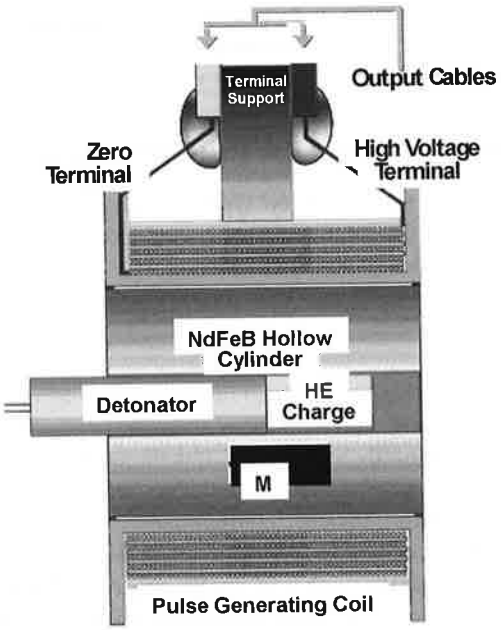

Fig. 3. Schematic diagram of a miniature transverse high-voltage FMG.[48]

the magnet. This changing magnetic field induces a current in a pickup coil around the magnet, which is then delivered to a load via a power-conditioning circuit. This type of generator can be used to deliver large currents to low-impedance loads.

- The SWG is a hybrid generator. The SWG uses the shock wave from an explosive charge to transition an electrically nonconducting material into an electrically conducting state within the shock front. Because shock waves tend to form rather thin layers, a thin metallization front is produced. This moving metallic layer takes the place of the metal armatures in FCGs and compresses the magnetic field to amplify the electric current. One of the potential benefits of this type of generator is that it may be able to eliminate Rayleigh–Taylor instabilities, which are encountered in conventional FCGs.

The FCG is a *field interaction*–type generator, whereas the FEG and FMG are *phase transition*–type generators. Obviously, SWGs fall into both of these categories.

The goal for all these generators is the same: deliver as much energy as possible to a load within a short period of time, called the *pulse duration*. Obviously, the shorter the pulse, the higher the power delivered to the load for a given amount of energy. Because the three parameters energy, pulse duration, and power are interrelated, only two of them are needed to classify these generators. Moreover, it is practical to limit oneself to just a single parameter, because the pulse duration is directly related to the speed of the explosives (typically millimeters per microsecond) and the size of the explosive generator. Herein, the energy delivered to the load per generator volume is chosen as the primary parameter, which can be converted for a given case into power by a rough knowledge of the pulse length. It is instructive to discern the *specific energy density*, which is the ratio of the energy delivered to the load to the active element volume, from the *system* or *demonstrated energy density*, which is the ratio of the energy delivered to the load to the entire volume of the

generator. It is generally understood by EPP researchers that they will have to address both the materials aspect, such as the specific energy density of the active element, and the applied physics/engineering aspect, such as size scaling of the entire generator.

4. Recent Advances in EPP Generators

As noted earlier, the development of new types of materials and sustained experimental programs have led to significant improvements in our understanding of EPP and, in some cases, breakthroughs in improving their performance.

4.1. FCG

There are several different variants of small FCGs, but they all operate on the same basic principle of compressing a magnetic field in an enclosed conducting volume or magnetic field flux trap. They differ primarily in the shape of their conductors, which is limited by the types of explosive initiation systems that are available. In other words, practical initiation systems may not exist for some geometric configurations.

In recent years, there have been two major advances in our understanding of the processes that take place in FCGs. First is the work done by Worsey et al.,[58] who conducted a detailed study of the fracture mechanics of armatures under shock loading. Second is that of Kiuttu and Chase,[21] who developed a resistance model for the contact point between the stator and armature. In addition, recent work has been done by Gilev,[14] Hemmert et al.,[16] and Freeman[11] on dielectric filled generators, i.e., SWGs, which may offer some advantages over classical FCGs.

4.1.1. Armature studies. While studying the propagation of the armature of an end-fired helical FCG, a new type of fracture formation was observed in the expanding armatures.[58] This observation helped to clarify the difference between simultaneously initiated radially driven armatures and end-fired axially propagating expanding armatures in conventional helical FCGs. As a result it became clear how to deal with this difference to offset some of the armature problems.

In addition to investigating the fracture mechanics of expanding armatures, Worsey et al.[58] investigate the effects of armature defects and explosive packing and voids on generator losses.

4.1.1.1. Armature fracturing. The armatures used in Ref. 58 were made of copper and aluminum and had a length of 15 cm, diameter of 3.8 cm, and wall thickness of 3 mm. The oxygen-free, high-conductivity copper cylinders were annealed to the soft state prior to testing, and the aluminum cylinders were tested in both their hard and soft states.

Examination of the high-speed photography of the expanding armatures revealed a previously unknown cracking on the outer surface of the armatures (Fig. 4). These cracks appeared in both types of metals, no matter their annealed state. These longitudinal cracks began on the surface of the armature at the detonator end of the cylinder and always stopped their extension at identical distances along the cylinders. Because the armature is part of the generator's electric circuit and the electric currents flow in a circumferential direction along its outer surface, it was thought that this might be one of the generator's loss mechanisms. In addition, the formation of cracks could introduce a loss of containment and result in magnetic flux losses. This cracking could also lead to arcing between the armature and the

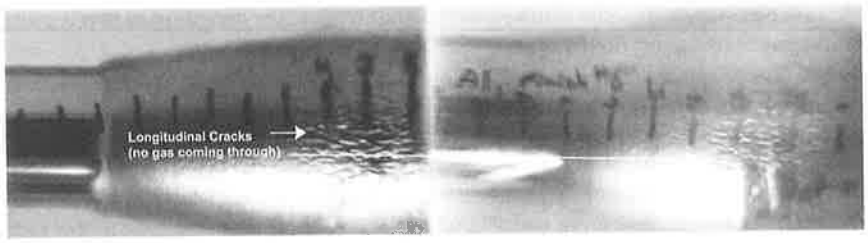

Fig. 4. Longitudinal cracking in expanding armature.

stator. This arcing could cause the stator insulation to break down before the sliding contact reaches the breakdown location, resulting in a high-resistance contact, i.e., the arc, between the armature and the stator, and the potential loss of magnetic flux. That is, the arcing causes the current flowing from the armature to the stator to jump ahead of the sliding contact, which is now no longer the current path. The magnetic flux trapped in the region between the sliding contact and the arc is lost to the compression process.

Metals tend to break when stressed beyond their strength limitations or when subjected to high strain rates. In the case of a metal cylinder, this limit is reached when it is expanded to more than twice its original diameter. It has long been known to researchers that the initiated end of the armature needed to be extended at least two diameters beyond the end of the stator for the generator to operate properly, but the reason was not well understood. Explosive expansion produces circumferential strains that can cause cracks that extend along the entire length of the armature. However, Worsey et al.[58] found that fracturing occurred much sooner than expected. In addition, they found that the fractures did not extend the length of the armature, as expected if they were purely the result of explosive expansion. This longitudinal fracturing occurred only within two diameters of the initiated end of the armature. Also, this fracturing occurred at much lower armature-diameter-expansion ratios than expected. Finally, they observed that normal explosive expansion fracturing begins on the inner surface, whereas the observed longitudinal fracturing occurs on the outer surface of the cylinder. It was concluded that this unusual longitudinal fracturing was not due to explosive expansion but rather some other effect: namely shock dynamics within the armature.

Some of the conclusions of the study (Ref. 58) were as follows:

- Shock wave and timing studies predicted that the cracks would form at the locations and times that were observed in the test.
- When the detonator is fired, a spherical detonation wave is formed. This causes the end of the armature to form a "bulb"-shaped structure rather than a propagating conical expansion plane. Geometric optics, applied to the detonation wave, indicates that the point where the detonation wave changes from spherical to semiplanar is the same place where the longitudinal fracturing stops.
- Mach stems, shock waves formed by the interaction of incident shock waves with reflected shock waves at the surface of the armature, were predicted to form in the region where longitudinal fracturing stopped. Mach stems alter the pressure distribution next to the explosive–armature interface, which causes the detonation wave to lose contact with the interface at about the same point the longitudinal fracturing stops.
- Hydrocode simulations indicate the presence of alternating periods of compression and tension within the armature in the region where the longitudinal fraction begins and that

the tensile stresses exceed the ultimate tensile strength of the armature in this region, thus forming crack-initiation points.
- These initiation points coalesce under low cycle fatigue, caused by these alternating stresses, and form incipient fractures.
- These incipient fractures open during explosive expansion and form premature cracking.

In summary, only detonation wave phenomena, such as transmission, reflection, refraction, and trailing rarefactions, are capable of producing incipient fractures at the locations and times when the cracking began on the outer surface of the armatures. The longitudinal fractures are caused by shock waves, not the expansion due to detonation. The expansion opens the fractures only once they are initiated.

4.1.1.2. Armature defects. For several decades there was an ongoing debate about the effects of armature surface defects on generator performance. The same cylinders used in the armature fracture study were used in an armature defect study.[5,6] Armature defect tests were conducted by using copper and aluminum armatures that had been polished and those that had rough finishes. It was found that the surface finish had little or no effect on the armature's expanding surface.

4.1.1.3. Explosive packing and voids. Because the C-4 explosives were hand packed in the experiments described above, there was concern about the uniformity of the explosive charge and the existence of voids. The explosive was hand loaded by using two methods. The first was to roll it into balls and then tamp the balls into the armature. This technique was thought to introduce cross-sectional voids and low-density regions within the charge. The second method was to form 2-cm disks and to push the disks into the armature. This method was thought to introduce mold line–type voids. To understand the impact of voids on generator operation, 4-mm-diameter spherical glass beads were introduced at various points within the explosive charge to simulate voids. In one set of experiments, the beads were placed along the charge–armature interface, and in another set they were inserted throughout the body of the explosive charge. The tests established that concerns about hand packing were unfounded, as long as care was exercised to ensure that added portions of explosive charge were knitted closely with previously loaded portions to prevent armature surface irregularities during expansion and that the only voids that appeared to affect armature expansion were those located at or near the explosive–armature interface.

4.1.2. Kiuttu contact point resistance model. One important characteristic of the helical FCG is its time-dependent electrical resistance. While developing a contact resistance model for the helical FCG, Kiuttu found an explanation for why small FCGs do not work as well as larger FCGs.

Kiuttu and Chase[21] developed a resistance model that includes diffusion and proximity effects for the armature–stator contact point. To develop this model, they developed an analytical expression that estimates the rate of magnetic field diffusion in the vicinity of the contact point. When converted to a flux loss rate, they found that it usually scales nonlinearly with the instantaneous current and that the resulting effective resistance is proportional to the square root of the current. Further, they found that the contact resistance generally increases throughout generator operation, even though the overall helical FCG resistance decreases as the generator length decreases. Finally, they found that the contact

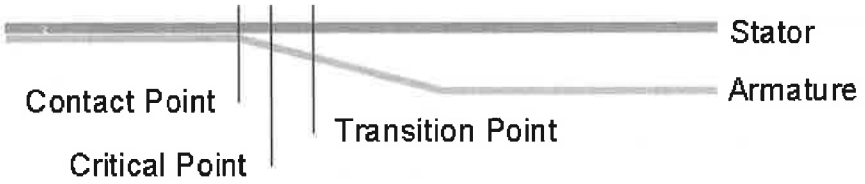

Fig. 5. Kiuttu and Chase divide the helical FCG into sections separated by two points: the critical point, where the local magnetic Reynolds number is unity, and the transition point, where the wire-to-wire proximity effect is equal to the wire-to-armature proximity effect.[21]

resistance usually dominates toward the end of generator operation and ultimately limits the gain of many helical generators, especially the smaller systems.

Kiuttu and Chase[21] postulated that there are three distinct regions (Fig. 5) in the vicinity where the armature makes contact with the stator. The first is the *transition point*. In the region downstream from this point, diffusion of flux into the stator is governed by the concentration of the field on the underside of the stator due to the wire-to-wire proximity effect. The *proximity effect* is where the wire-to-wire interactions in the stator or the stator-to-armature interaction as the armature approaches the stator alter the magnetic field and current density distributions that initially existed before the arrival of the contact point. These nonuniform magnetic field distributions around the wire increase the resistance. The second point is the *critical point*, which is the point ahead of the contact point that defines the region where most of the flux behind it diffuses into the conductors and most the flux ahead of it is advected ahead toward the load. They further postulated that if the flux per unit length in the armature–stator gap at the critical point could be determined and that if it would then be multiplied by the critical point velocity, then the effective voltage and, thus, the resistance across the generator at that point can be found. The three parameters that must be found are the location of the critical point, its velocity, and the flux per unit length at that point.

To find the location of the critical point, they introduced the magnetic Reynolds number. It is a dimensionless quantity that relates the relative importance of flux advection to that of diffusion and is defined to be the ratio of the time to move flux over a given distance in vacuum to the time it takes for it to diffuse the same distance into a resistive medium. In other words, the critical point is the point at which the rate of flux diffusion into the conductor just equals the rate at which the flux is pushed ahead of the armature and its magnetic Reynolds number is defined to be equal to one.

Because the distances between these three points are very small, there are strong armature–stator proximity effects that make the surface fields very strong, thus causing nonlinear diffusion. The contact point resistance is nonlinear and scales as the square root of the current. It depends weakly on the properties of the materials used to construct the generator and the armature expansion angle. This model appears to give good results when applied to small- and medium-sized simple helical FCGs and has been incorporated into the CAGEN 1 1/2-D modeling code for helical FCGs.

All of the current computer models currently use empirically adjustable factors to model FCGs. These factors are not universal and must be empirically adjusted for each FCG design and for different operating parameters. The Kiuttu formulation is universal for helical FCGs, because there are no adjustable factors and it accurately calculates output current to within 20% of experimental values.

4.1.3. SWGs. SWGs are very similar to FCGs, with the exception that magnetic field compression occurs within a solid material, rather than in a gas. Several undesirable processes can affect the operation of conventional helical FCGs, including instabilities, e.g., Rayleigh–Taylor, and multiple loss mechanisms such as 2π-clocking, i.e., flux losses caused by turn skipping of the contact point due to armature–stator misalignment, nonlinear diffusion, and so on. It has been proposed that these instabilities and loss mechanisms can, at least partially, be eliminated by compressing the FCG's magnetic flux in solids such as ionic salts, semiconductors, or oxide-coated aluminum powders. This is accomplished through a process that shock transitions a dielectric into a metallic state or that fractures the oxide coatings on metallic powders. When a shock wave passes into these materials, it transitions the material inside the shock front into the metallic state. This propagating metallic shock front takes the place of the metallic armature in conventional FCGs.

In the early 1960s, it was found that certain dielectrics, such as silicon, and oxidized metallic powders become electrically conducting under static and shock compression. It was found that under static compression, the electrical conductivity of silicon increases monotonically with increasing pressure and eventually reaches the conductivity of classic metals. In addition, it was found that shock compression of silicon causes metallization to occur when the silicon's Hugoniot elastic limit is exceeded. The difference between static compression-induced conductivity and shock-induced conductivity in silicon is that the shock conductivity was found to be six orders of magnitude greater at a pressure of 15 GPa. Other substances that exhibit this property are germanium, selenium, gray tin, silicon oxide, cesium iodide, germanium iodide, and lithium niobate ($LiNbO_3$).

Possible advantages of SWGs over conventional FCGs are as follows:

- Practically complete compression of the magnetic field within the working volume.
- Freedom from instabilities, such as Rayleigh–Taylor instabilities, associated with the imploding liner in conventional FCGs.
- Faster operation, which is determined by the shock velocity.

In recent times, there have been a number of theoretical and experimental advances in our understanding of SWGs. Some recent theoretical advances are as follows:

- Kolosenok et al.[22] reported that shock wave compression of magnetic fields in solid materials is not as strongly limited by magnetic pressure as it is in conventional FCGs. For example, Hemmert et al.[15] reported that one can compress magnetic fields in aluminum powder even when the magnetic pressures generated by the compression process are an order of magnitude greater than the amplitude of the shock waves driving the flux compression.
- Velikovich[57] has reported that electrical breakdown in the uncompressed material ahead of the shock wave may be a more restricting condition in the operation of SWGs.
- Investigations by Barmin and Prischepenko,[7] Kolosenok et al.,[9] and Tracy et al.[56] of CsI monocrystals and by Bichenkov[9] of powders suggested that when the shock wave converges toward the center of an imploding SWG, the ionized shock front decelerates and transitions into an oscillatory compression mode, i.e., the pressure, material density, and local magnetic flux density oscillate behind the shock front.

Some recent experimental advances are as follows:

- While investigating shock-induced changes in the electrical conductivity of aluminum powder in closing switches for ultracompact explosive generators such as FEGs, Hemmert

found that the change in conductivity is independent of grain size but may be influenced by the method used to pack the powder. In other words, the gain of SWG is related to the porosity of the Al powder.

- Hemmert et al.[16] also found that high-voltage hold-off tests showed a large difference in hold-off capabilities for different grain sizes, with the larger grains performing the worst. They concluded that the use of aluminum powder in compact explosive closing switches appeared possible for low-voltage applications and that the use of nanopowders may achieve higher hold-off voltages.

In addition to the recent experiments done by Hemmert and his colleagues, Gilev[13] has also reported on some of his recent experimental findings. Gilev pointed out that current models for SWGs are based on a number of assumptions: (1) the material is incompressible, (2) the electrical conductivity increases just behind the shock front but does not change later, (3) the electrical conductivity does not depend on pressure, and (4) the electrical conductivity is very high so that magnetic diffusion losses from the uncompressed region are negligible. In other words, these models do not take into account the compressibility of the material, shock-induced metallization, effects due to magnetic compression, shock dynamics, and so on. To account for these shortcomings, Gilev developed a magnetoelectrical experimental technique for studying insulator–metal transitions under shock compression. Some of the results from his studies are as follows:

- The thickness of the skin layer of coarse powders is smaller than the thickness of the shock transition zone, which implies that magnetic compression is effective in only fine powders, not coarse powders.
- Metallization of aluminum powder occurs only within the shock front and not in an elastic precursor proposed by Novac et al.[26] In fact, Gilev saw no evidence[13] of the precursor wave being formed, which is in agreement with two-dimensional hydrodynamic simulations done in the United States.
- The electrical conductivity of silicon and selenium increases by 5 and 12 orders of magnitude, respectively, without a noticeable delay (within a few nanoseconds) under shock compression.
- The pressure dependency of electrical conductivity consists of two parts: a steep rise in conductivity followed by a plateau. The plateau conductivity corresponds to that of the metallic state. This plateau regime does not depend on the type of doping or impurities that may be present. The metallic state tends to be metastable in that when the stress is released there is a temporary delay in the reverse transition.
- The threshold pressure for metallic transition in silicon is about 10 GPa, and metallization occurs at approximately 12 GPa.
- Metallization in solid selenium occurs at about 21 GPa. Powdered selenium undergoes metallic transition at a lower pressure than does solid selenium.
- As the shock pressure increases in powdered aluminum, its conductivity increases sharply, reaches a maximum, and then decreases. This behavior reflects the combined effects of compression and heating by the shock wave.

These recent discoveries are important to the development of SWGs. However, they alone do not ensure that magnetic flux compression is really feasible in solid and powder dielectrics and metal oxides. Bichenkov[9] and Gilev[13] have investigated this question as well. In experiments conducted by Gilev, he generated a converging metalized shock wave in aluminum powder immersed in an external magnetic field. He measured a magnetic field

amplification of $B/B_0 = 39$, where B_0 is the initial magnetic field and B is the compressed magnetic field in the SWG.

In summary, Hemmert, Gilev, and others have recently demonstrated that shock wave compression of magnetic fields in solids is feasible, determined that using powder dielectrics is better than using solid dielectrics, and determined that particle size and porosity are important parameters.

4.2. FEG

The first paper describing explosive-driven FEGs was published by Nielsen[24] in 1957. It was demonstrated for the first time that shock-compressed lead zirconate titanate (PZT) and barium titanate ferroelectric materials are capable of generating high-voltage and high-current pulses.[24] Throughout the 1960s and 1970s, shock depolarization of ferroelectric materials was intensely studied at Sandia National Laboratory (SNL) and the Naval Surface Weapons Center. Detailed experimental studies of shock depolarization of a variety of ferroelectric materials were performed using precisely calibrated planar shock waves generated by projectiles accelerated in light-gas guns or by specially designed explosive lenses. During this period, a few theoretical models were developed based on the available experimental data. Research on shocked ferroelectric materials declined throughout the 1980s and early 1990s, until it was revived in the late 1990s by SNL.[31]

In the late 1990s, Shkuratov et al. and Tkach et al. at Texas Tech University (TTU)[32,55] began a systematic investigation of miniature explosive-driven FEGs. This work was continued by Shkuratov et al.[39,40,42,43,50] and Baird and Shkuratov[3] at Loki, Inc., and by Holt et al. at HEM Technologies.[17]

Loki focused on research and development of miniature highly efficient explosive-driven FEG that are capable of operating with different types of electrical loads. These generators were developed under the restriction that they had to be as small and as light as possible. Owing to their small size, the shock waves generated in explosive-driven FEGs are not perfectly planar. This results in a much more complex electrical response by the shock-compressed ferroelectric modules in miniature FEGs in comparison with that obtained in those experiments in which planar shock compression was generated by gas gun projectiles. This led to the necessity of performing detailed experimental studies, understanding the results of these experimental studies, and development of sophisticated theoretical models for each specific FEG design.

Since 2004, Loki, Inc., has conducted more than 400 explosive-driven FEG experiments. As a result, Loki developed several different reliable miniature FEG designs. The first successful design was based on longitudinal depolarization of PZT materials.[39,40,42,43,50] Longitudinal depolarization occurs when the shock wave propagates along the polarization vector of the ferroelectric element. Other FEG designs, which were even more effective than the longitudinal design, were also investigated. One of these new designs was based on transverse depolarization of ferroelectric materials (see Fig. 2; Loki, Inc. patent pending[3]). Transverse depolarization occurs when the shock wave propagates perpendicular to the polarization vector of the ferroelectric element.

Loki, Inc., used its longitudinal FEG design[50] as a basis for research and development of a series of high-voltage, multiple-cycle piezoelectric generators. Loki, Inc., also developed a compressed-air–powered piezoelectric generator of diameter 50 mm and length 250 mm that is capable of producing an unlimited number of high-voltage pulses with amplitude

Fig. 6. Typical miniature Loki explosive-driven, 140-kV FEG.

up to 110 kV. At present, Loki, Inc., in cooperation with Farr Research, has successfully developed miniature high-power microwave (HPM) systems based on a Loki FEG.

Loki, Inc., has developed FEGs to the point that they can reliably and consistently generate voltages in excess of 130 kV from a device with a diameter of 38 mm and a length that ranged from 55 to 90 mm. A photograph of a typical Loki FEG is shown in Fig. 6. One of their most significant findings is that these generators can generate multiple cycles despite being single-shot devices.

Some of the recent advances in FEGs are the identification of the following:

- New ferroelectric materials with higher energy storage densities and higher electric breakdown thresholds that significantly increase the output voltage of the FEG.
- New potting materials that yield good electrical, mechanical, and shock properties.
- Improved power-conditioning techniques that yield optimal output voltages and provide better impedance matching with a variety of loads.

The most significant improvement in FEGs is due to advances in ferroelectric ceramics. TRS Technologies, under a Small Business Innovative Research program, developed and refined a process for producing quantities of PZT 95/5 for shock wave experiments. HEM Technologies, working with TRS, proved that TRS's PZT 95/5 material clearly outperforms the more traditional PZTs (EC-64 and TRS100) in charge release (Fig. 7), while maintaining a similar dielectric strength (Fig. 8).[17]

Replacement of PZT EC-64 with the same-sized 95/5 elements resulted in a dramatic (more than double) increase in the output voltage. Typical output voltage waveforms produced by Loki FEGs containing PZT EC-64 and PZT 95/5 samples are shown in Fig. 9. The dependence of the output voltage produced by FEGs on the thickness of PZT elements for both PZT EC-64 and PZT 95/5 is shown in Fig. 10.

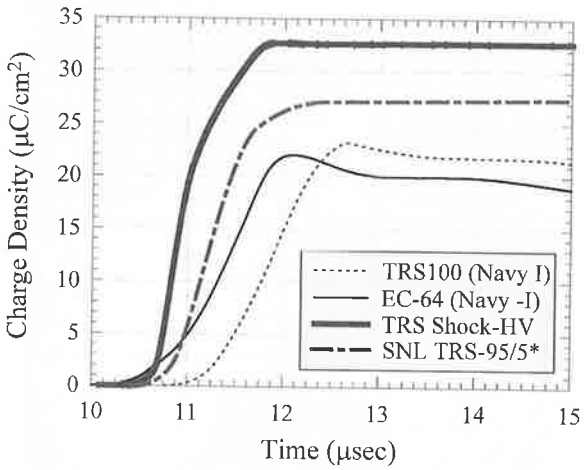

Fig. 7. Comparison of the charge density for various formulations of PZT.

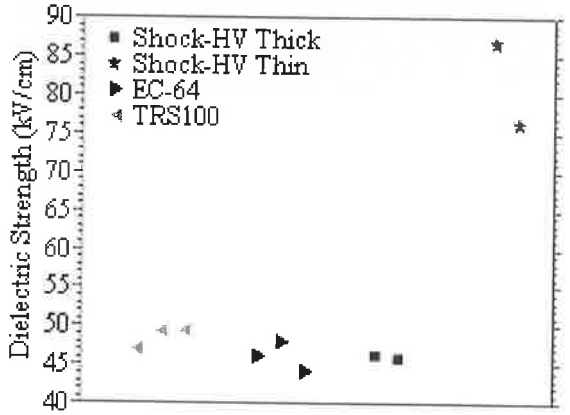

Fig. 8. Dielectric strength measurements by TRS Technologies of different types of PZT used in FEGs.

From their systematic study of FEGs, Loki, Inc., observed the following trends:

- The profile of the shock wave significantly affects the amplitude of the output voltage and current pulses produced by both longitudinal and transverse FEGs. Changing the shock wave profile leads to an increase (or decrease) in the amplitude of the output voltage pulses by a factor ranging up to 2.4 for both types of FEGs with the same PZT elements.
- For FEGs operating with high resistive loads, the amplitude and full-width half-maximum (FWHM) of the voltage pulse produced by FEGs are highly reproducible and increase as the thickness of the PZT element increases (Fig. 10). In addition, increasing PZT thickness increases the energy produced by the FEG but reduces the specific energy density stored in the PZT.
- For FEGs operating with resistive loads, the amplitude of the output voltage increases noticeably as the resistance increases. However, the amplitude of the current pulse decreases as the resistance increases (Fig. 11). The power and energy transferred to the load increase up to a certain load resistance, after which they decrease.

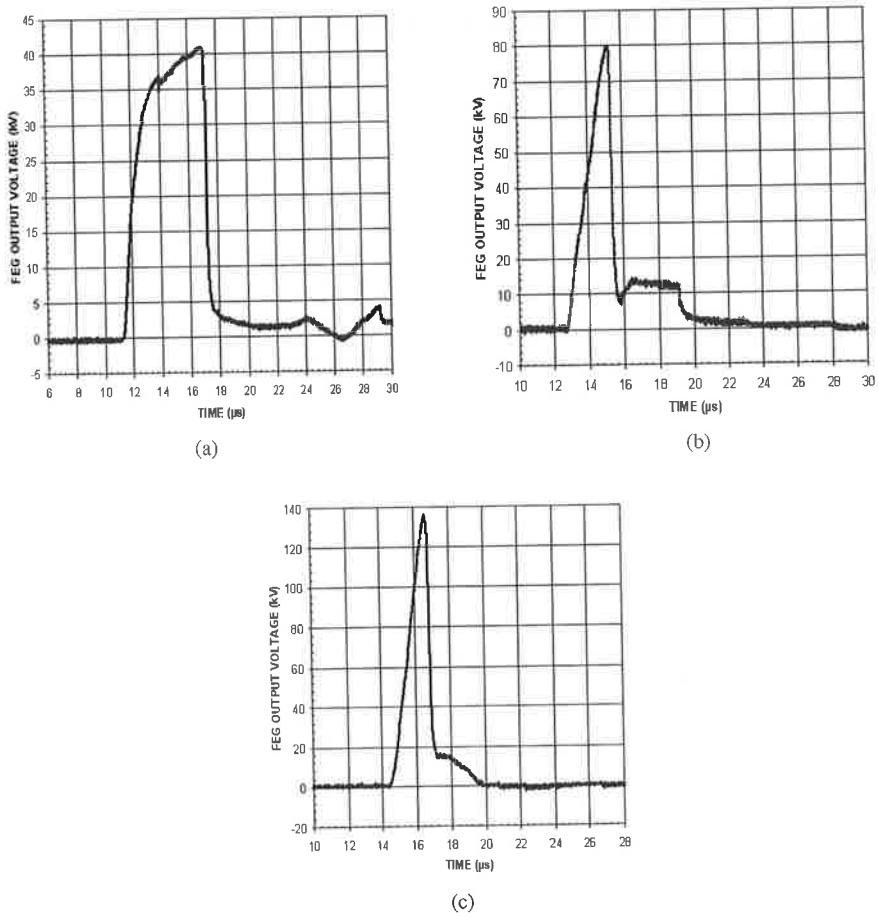

Fig. 9. Comparison of the output voltage produced by FEGs containing $Pb(Zr_{0.52}Ti_{0.48})O_3$ (PZT EC-64) and $Pb(Zr_{0.95}Ti_{0.05})O_3$ (PZT 95/5) elements. (a) PZT EC-64 bar with dimensions of 12 × 12 × 50 mm. (b) PZT 95/5 bar with dimensions of 12 × 12 × 50 mm. (c) PZT 95/5 cylinder of diameter 20 mm and length 26 mm.

- For FEGs operating with capacitive loads, the amplitude of the voltage pulse decreases as the capacitance increases (Fig. 12). However, the electric charge transferred to the load increases as the capacitance increases. The energy transferred to the load increases up to a certain load capacitance, after which it decreases.
- Certain ferroelectric and potting materials and certain ferroelectric element shapes are better than others for yielding high output voltages. As an example, Loki shot single-element generators with rectangular EC-64 and PZT 95/5 elements and one with a cylindrical PZT 95/5 element. The latter provided significantly higher voltages (Figs. 9 and 10). A comparison of the effects of various potting compounds on the output of the FEG was also studied, and the results are presented in Fig. 13.

In summary, Loki, Inc., is now in a position to supply FEGs to commercial customers. These generators are highly reliable and can consistently generate high voltages. It was recently demonstrated by Loki, Inc., that their FEGs can be considered to be robust,

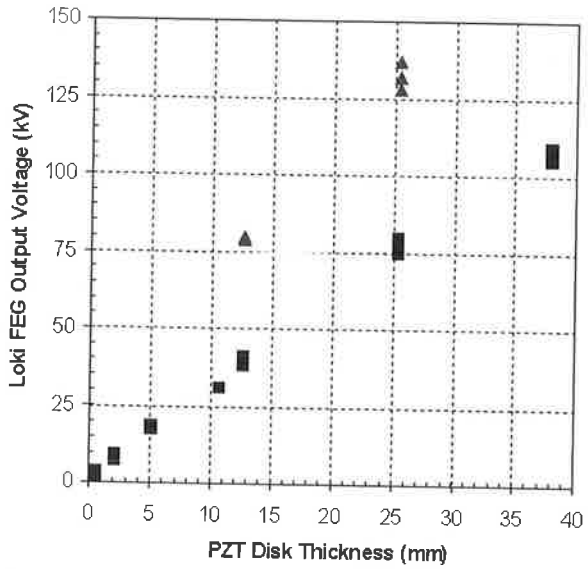

Fig. 10. The amplitude of the output voltage pulses produced by FEGs versus the thickness of $Pb(Zr_{0.52}Ti_{0.48})O_3$ (PZT EC-64) (squares) and $Pb(Zr_{0.95}Ti_{0.05})O_3$ (PZT 95/5) (triangles) ferroelectric elements. The FEG output voltage is directly proportional to the thickness of the ferroelectric modules.

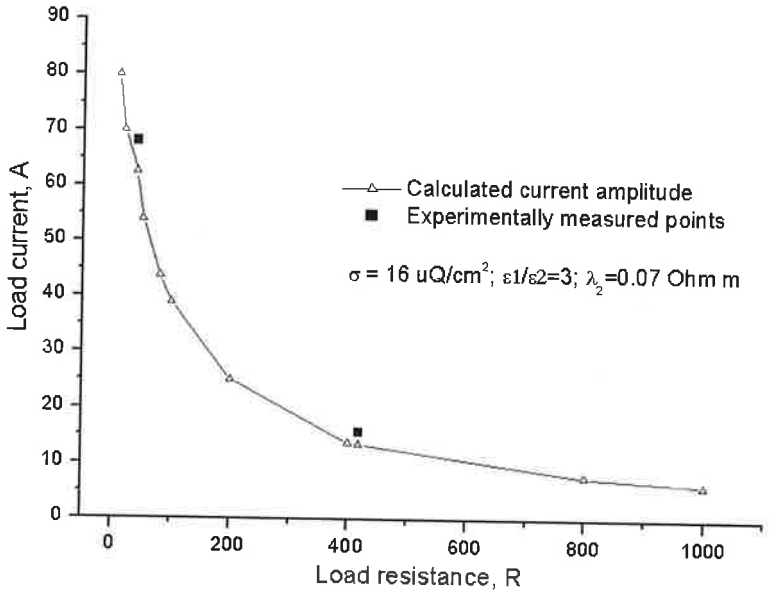

Fig. 11. The current in the active load decreases as the load resistance increases. The reason for this is the increase in the losses in the shock-compressed portion of the PZT module due to bulk leaks stimulated by the shock wave. Both the theoretical and experimental results suggest that the longitudinal FEG can be effectively treated as a current source until the load resistance begins to approach the shunt resistance of the shock-compressed portion of the PZT module.

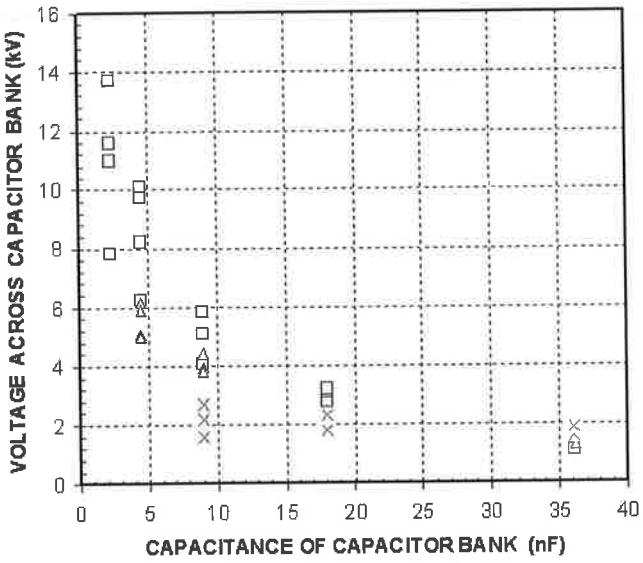

Fig. 12. FEG-capacitor bank experiments were performed using a wide range of capacitances, from $C = 2.25$ nF to $C = 36$ nF. This figure summarizes data for all the FEG-capacitor bank systems studied. The experimental data for FEGs containing $Pb(Zr_{52}Ti_{48})O_3$ disks with $D = 27$ mm/$h = 0.65$ mm are marked by crosses ($\times$); data for FEGs containing $Pb(Zr_{52}Ti_{48})O_3$ disks with $D = 27$ mm/$h = 2.1$ mm are marked by triangles ($\triangle$); and data for FEGs containing $Pb(Zr_{52}Ti_{48})O_3$ disks with $D = 27$ mm/$h = 5.1$ mm are marked by squares ($\square$).

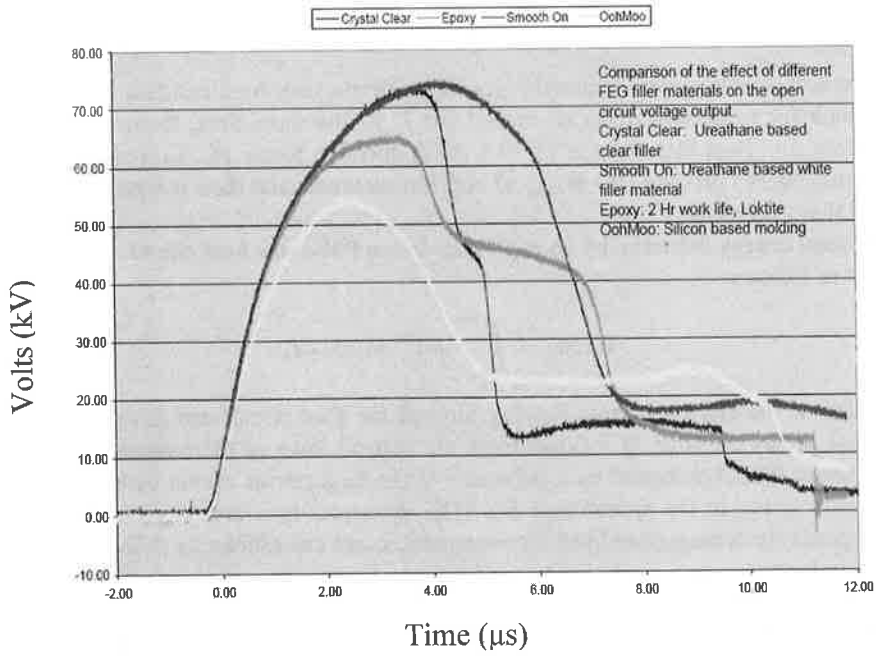

Fig. 13. Comparison of the measured open-circuit output voltage of EC-64 and PZT 95/5 and different geometrical configurations for PZT 95/5.

high-power prime power sources for miniature HPM systems. If a quick estimate of FEG performance is needed, one can mathematically describe the FEG as a pulsed current source with nearly constant current amplitude. Hence, the energy transferred to the load, i.e., the specific energy density, is dependent on the load itself. For instance, a specific energy density of 1,000 mJ/cm^3 or system energy density of 11 mJ/cm^3 has been reported for an FEG firing directly into a resistive load.

4.3. FMG

The first paper describing pulsed-power generation by explosive-driven electrical transducers based on the shock wave demagnetization of ferromagnetic materials was published by Kulterman et al. in 1958.[23] Their generator[23] was based on the demagnetization of a closed soft ferromagnetic core by shock waves generated by an accelerated projectile.

Two important principles limit the utility of the generators described in Ref. 23 and determine whether FMGs can be used as prime pulsed-power sources:

- The generators in Ref. 23 were not autonomous sources of prime power. Their closed soft ferromagnetic core had to be magnetized to saturation immediately before explosive operation. Therefore, an exciting electric current generated by electrochemical batteries was passed through the generating coil in Ref. 23. Thus, these FMGs require a seed source.
- The electromagnetic energy density that can be stored by soft ferromagnets is extremely low. Indeed, the magnetostatic energy E stored in a magnetized body can be expressed as a volume integral of the scalar product $(\mathbf{B} \cdot \mathbf{H})$ taken at each point in the magnetic medium:

$$E = -0.5 \iiint_V (\mathbf{B} \cdot \mathbf{H}) \cdot dv. \tag{1}$$

Most soft ferromagnetic materials typically possess very high residual magnetization, B_r, which for some materials can exceed 2.0 T. At the same time, these materials have extremely low (less than 1.0 Oe or 79.5 A/m) coercive force, H_c. Correspondingly, the maximum energy product $(\mathbf{B} \cdot \mathbf{H})_{\max}$ of soft ferromagnets and their magnetostatic energy [Eq. (1)] are very low.

The total energy delivered by an explosive-driven FMG to a load circuit, $W(\infty)$, can be written as follows:

$$W(\infty) = \int_0^{+\infty} I(t) \cdot U(t) \cdot dt, \tag{2}$$

where $I(t)$ is the electric current flowing through the load circuit and $U(t)$ is the electric potential across the load. It follows from the general laws of thermodynamics that the total energy $W(\infty)$ delivered by a generator to the load circuit cannot exceed the energy E initially stored in the system [see Eq. (1)]. However, there are no grounds to believe that explosively demagnetized soft ferromagnetic cores can efficiently deliver their stored energy to loads.

In the late 1990s, Shkuratov et al.[44–49] and Talantsev[54] at TTU proposed and began investigating the use of hard ferromagnetic materials. Hard ferromagnets possess significantly (up to two times) lower residual magnetization B_r than the best soft ferromagnetic

materials. At the same time, the coercive force of hard ferromagnets is from four to eight orders of magnitude higher than that of soft ferromagnets. Correspondingly the maximum energy product $(\mathbf{B} \cdot \mathbf{H})_{max}$ and, consequently, the magnetostatic energy [Eq. (1)] stored in hard ferromagnets are at least four orders of magnitude higher than those of soft ferromagnets. The maximum energy product for commercially available hard ferromagnetic materials can be as high as $(\mathbf{B} \cdot \mathbf{H})_{max} = 0.4$ J/cm^3.

Hard ferromagnets have one more important advantage in comparison to soft ferromagnetic materials. A hard ferromagnet does not require a seed source to magnetize it prior to explosive and electrical operation of the FMG. It is a completely self-contained system. Pulse-generating systems based on hard ferromagnets can be smaller, lighter, and simpler than those based on soft ferromagnets.

Even though hard ferromagnets store a large amount of magnetostatic energy, this does not mean that this energy can be released due to shock wave action in an explosive-driven FMG. Thus a study was undertaken to find hard ferromagnetic and ferrimagnetic materials that can be demagnetized by shock wave compression.

Experimental investigations of shock-induced phase state transitions in hard ferrimagnets and ferromagnets were performed by Shkuratov et al.[44–49] and Talantsev et al.[54] at TTU in the late 1990s, 40 years after the initial investigations of shock-induced magnetic phase transitions in soft ferromagnetic materials.

As a result of this study, it was demonstrated that high-energy hard ferrimagnets ($BaFe_{12}O_{19}$) and ferromagnets ($Nd_2Fe_{14}B$) do undergo ferrimagnetic/ferromagnetic-to-paramagnetic phase transitions due to longitudinal shock compression, i.e., where the shock wave propagates along the magnetization vector **M** (Refs. 44, 46, and 49). This physical effect formed the basis for the development of a new type of explosive-driven prime power source, i.e., the modern FMG.[44,46,49]

After 2 years of investigating longitudinal shock wave compression of hard ferrimagnetic and ferromagnetic materials, Shkuratov et al.[45,47] at TTU began investigating transverse, i.e., when the shock wave propagates perpendicular to the magnetization vector **M,** shock wave demagnetization of $Nd_2Fe_{14}B$ hard ferromagnets. Transverse shock demagnetization of hard ferromagnets led directly to a new way to design really small high-current and high-voltage FMGs.[45,47,48,54]

Since 2004, Shkuratov and Baird have continued systematic studies of shock wave FMGs at Loki, Inc., and have conducted more than 450 shots. A variety of FMGs were designed, constructed, and tested. As a result of these efforts, they have developed several very reliable compact high-voltage and high-current FMG designs that provide consistent outputs[33–38,53] (patent pending[4]). These generators are now commercially available from Loki, Inc.

The schematic diagram of an ultracompact high-voltage pulsed generator based on transverse shock wave demagnetization of $Nd_2Fe_{14}B$ ferromagnets developed by Loki, Inc.,[33] is shown in Fig. 3. It contains an $Nd_2Fe_{14}B$ hollow ferromagnetic cylinder magnetized along its axis, with an explosive charge loaded in the central hole and a pulse-generating coil wound on the ferromagnet.

Upon the detonation of the explosive charge, a transverse shock wave is generated. The shock wave propagates through the body of the ferromagnetic element (Fig. 3) perpendicular to the magnetization vector **M** and demagnetizes it. The magnetic flux inside the pulse-generating coil decreases, due to the shock demagnetization of the $Nd_2Fe_{14}B$ element. In accordance with Faraday's law, a pulsed electromotive force (EMF) is generated at the output terminals of the FMG. For a multiturn coil (Fig. 3), the EMF generated is the sum

of the EMFs produced by each of the turns:

$$\mathrm{EMF}_{m-\mathrm{turn}}(t) = \sum_{N} [-\mathrm{d}\Phi_n(t)/\mathrm{d}t], \tag{3}$$

where $\mathrm{d}t$ is the time it takes the magnetic flux in the turn to change, $\mathrm{d}\Phi_n(t)$ is the magnetic flux captured by the nth turn of the multiturn coil, and N is the number of turns in the coil.

FMGs have an advantage over FEGs and FCGs in that there is no direct electrical connection between the ferromagnetic element and the pulse-generating system of the device. The ferromagnet is electrically insulated from the pulse-generating system, and there is a transformer-type coupling only between the ferromagnet and the pulse-generating coil. Therefore, the pulse-generating coil of the FMG is not subjected to explosive shock during demagnetization, which means that its electrical parameters do not change during electrical operation. This made it possible for Talantsev et al.[53] to develop analytical techniques for calculating the currents produced by explosive-driven FMGs.

FMGs may be classified as being either high-current (kiloamperes) or high-voltage (kilovolts) sources. Increasing the number of turns in the pulse-generating coil of the FMG increases its output voltage (at the same time it increases the impedance of the pulse-generating coil). Thus, a single-turn or low-turn FMG is a high-current source, and a multiturn FMG is a high-voltage source.

A typical high-voltage pulse produced by a transverse FMG having a diameter of 3.0 cm (total volume 18 cm^3) is shown in Fig. 14(a). Figure 14(b) shows the output voltage of the same FMG versus the number of turns in the pulse-generating coil.[33] It follows from experiments that as the number of turns in the pulse-generating coil increases, the peak amplitude of the voltage pulse increases proportionally [Fig. 14(b)].

It has been experimentally determined that FMGs reliably generate high-voltage pulses with a pulse length of about 20 μs, which is sufficient time for charging capacitor banks[33] or powering vector inversion generators.[34]

Loki proposed and experimentally verified a new concept for constructing compact autonomous multistage FMGs.[36] This pulsed-power system consisted of identical ferromagnets connected to each other in series or in parallel. A schematic diagram of this multicell system is shown in Fig. 15(a). The waveforms of output voltage produced by separate FMG cells and by the multistage system are shown in Figs. 15(b) and 15(c).[36]

A photograph of a Loki high-current FMG of diameter 5.1 cm and total volume 25 cm^3 is shown in Fig. 16(a). The waveform of the current pulse produced by this high-current FMG is shown in Fig. 16(b). The peak amplitude of the current pulse was 4.45 kA, and its rise time was 28 μs (Ref. 48). The ability of the high-current FMG to produce relatively long current pulses (Fig. 16) is another important advantage of these devices, thus making them good seed sources for FCGs. It was experimentally demonstrated by Loki that when the diameter of the $Nd_2Fe_{14}B$ ferromagnetic element increases, the peak amplitude of the current pulse increases.[38,48]

In summary, a new type of explosive-driven prime power source based on shock demagnetization of hard ferromagnets was developed. Commercially available FMGs developed by Loki, Inc., are very reliable, inexpensive, simple to operate, and capable of producing both high voltages and high currents. The specific energy density of these devices varies from 30 to 60 $\mathrm{mJ/cm}^3$, depending on the type of load used. It has been experimentally shown that these generators can be effectively used as seed sources for FCGs,[37,38,54] prime power sources for charging spiral vector inversion generators,[34] and prime power sources for charging capacitor banks.[33]

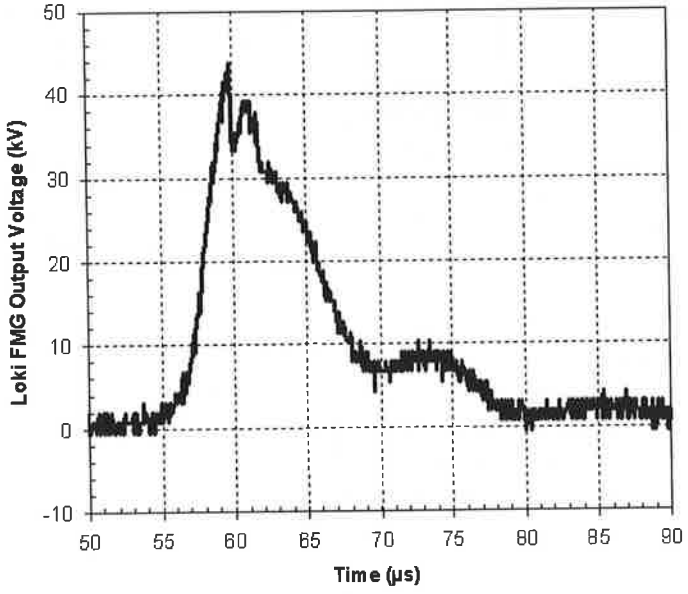

(a)

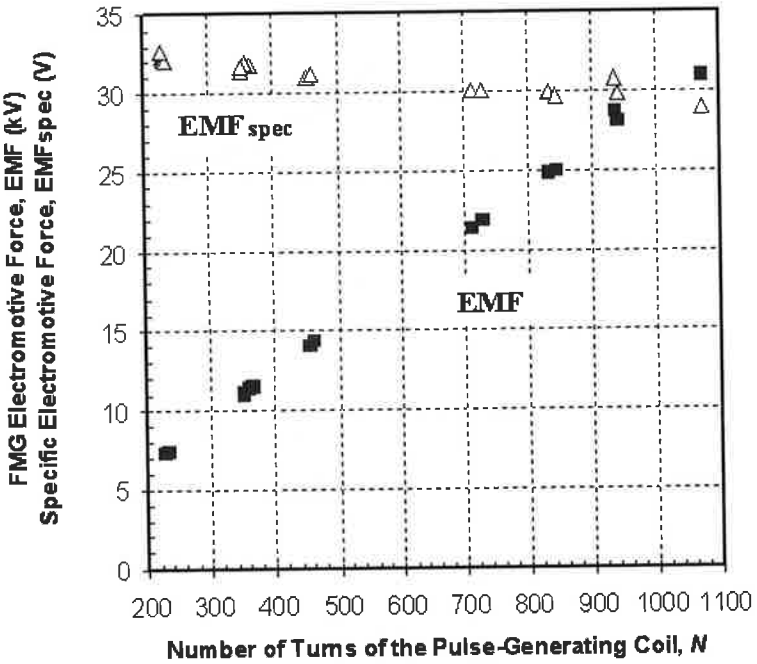

(b)

Fig. 14. (a) Typical waveform of the output voltage produced by Loki's FMGs. (b) The peak amplitude of the output voltage produced by high-voltage FMGs and the specific voltage per turn versus the number of turns in the pulse-generating coil. The FMG output voltage is directly proportional to the number of turns in the pulse-generating coil.

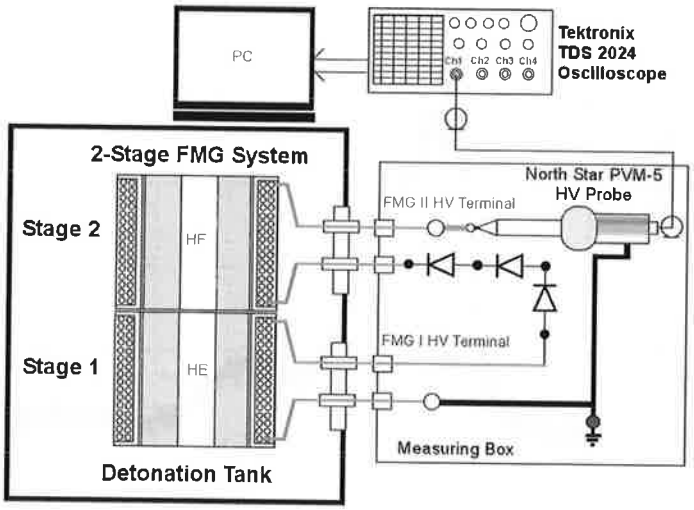

(a)

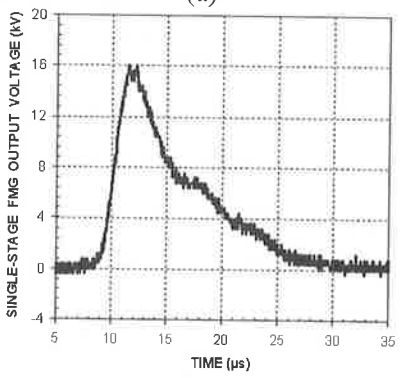

(b)

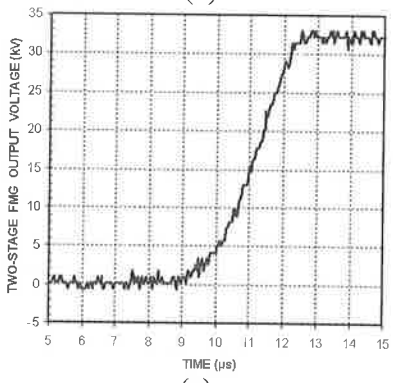

(c)

Fig. 15. (a) Schematic diagram of a two-cell FMG pulsed-power system. Typical waveforms of the high-voltage pulse produced (b) by a single-stage and (c) by a two-cell FMG (423-turn pulse-generating coils). The amplitude of the voltage pulse produced by the (c) two-cell FMG was $U(t)_{\max} = 32.0$ kV, which is twice the output voltage produced by a (b) single-stage FMG system, and its rise time was $\tau = 3.5$ μs.

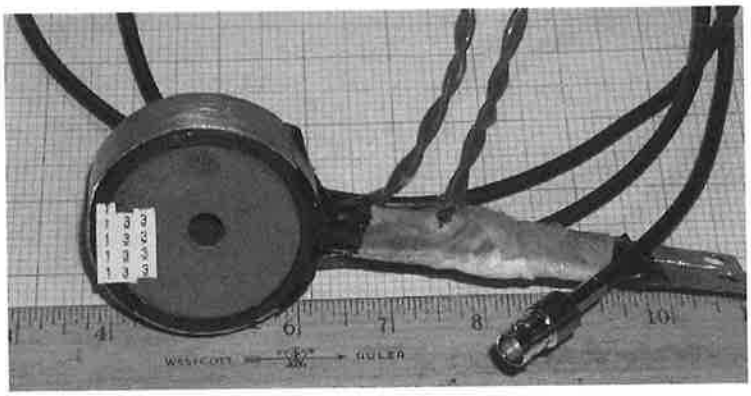

(a)

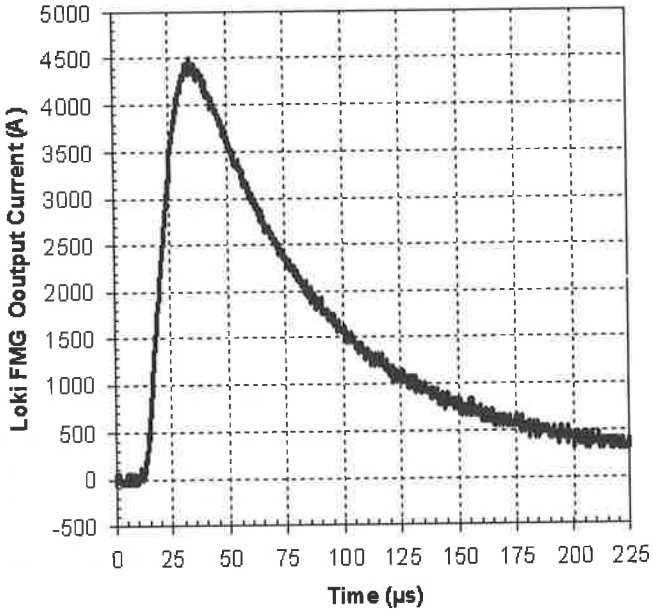

(b)

Fig. 16. (a) Single-turn FMG used to seed FCGs and (b) typical waveform of the current pulse produced by this FMG.

5. Seed Sources and Power Conditioning

The FEG and FMG are self-contained in that they do not require a seed source, unlike the FCG and SWG, which do require one. Of course, all four generators do require fuzing systems and power-conditioning circuits.

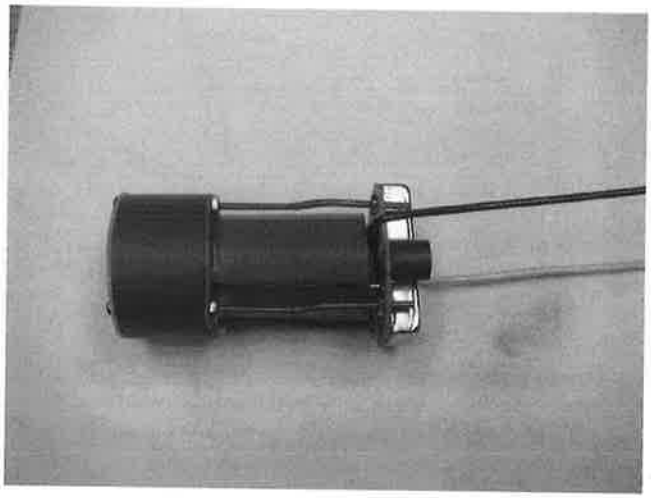

Fig. 17. Battery-powered seed source developed by HEM Technologies for small- and medium-sized FCGs. The energy density is roughly 30 mJ/cm^3.

5.1. Seed sources

All FCGs require that an initial (or seed) magnetic field exist within the working volume of the generator. It is this initial field that the FCG amplifies. There are two methods for seeding FCGs. The first method is *direct seeding* by which the initial field is established by using the FCG geometry. This is accomplished by passing an electric current through the generator circuit and inducing the initial field in the FCG working volume. The second method is *indirect seeding* by which the initial magnetic field is established within the working volume of the FCG by using either permanent magnets or an external coil that is not part of the FCG circuit.

The typical seed sources used in most FCG experiments are capacitor banks, because helical FCGs are inductive circuits and a capacitive discharge circuit is a natural choice. However, over the years several relatively successful attempts have been made to use batteries, FEGs, FMGs, external electromagnets, and external permanent magnets as seed sources. There have been recent advances in using some of these other compact seed sources by TTU, HEM, and Loki. We will briefly discuss the HEM and Loki seed sources in this section and the TTU seed source in the next section.

HEM Technologies developed a very compact battery-powered seed source (Fig. 17). Assuming a 10-μH load, the seed source was designed to deliver a peak output current of >1 kA. The components of this seed source are batteries, a 20-μF capacitor capable of storing 10 J, a dc–dc converter with 1-kV output, and a switch. This seed source had a diameter of 5 cm and a height of 10 cm. It was demonstrated that this seed source could deliver in excess of 1 kA to an inductive load. Or more important, the system energy density, defined as the ratio of the energy delivered to the load to the system volume, was ~30 mJ/cm^3. It is believed that its volume can be decreased by 25% and its output current increased, provided that the components are specifically engineered for the space allotted.

Loki has done considerable work on using FMGs as seed sources for two types of FCGs, namely the helical FCG[34,35,38,54] and the loop FCG.[37] One version of the seed source was a single-turn, high-current FMG. The FMG was made by using magnets with an outside

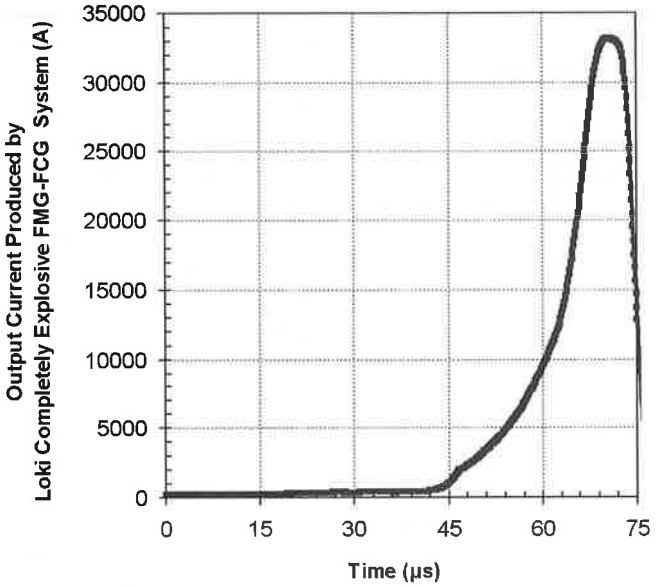

Fig. 18. The output current produced by an FMG-seeded helical FCG system. The output current amplitude was 33.6 kA, and the rise time was 26 μs. In this experiment, a current (energy) amplification factor of 112 was achieved into a 100-nH load.[55]

diameter of 50 mm and a length that ranged from 13 to 100 mm. Note that whereas FMGs have reached specific energy densities of 40–50 mJ/cm^3, the system energy density is lower than that, depending mostly on the FMG design. FMGs using only a few grams of HE have shown the most promise.

Loki has developed both single-magnet and multiple-magnet FMGs to seed FCGs. The FMG seed source has been both directly[38,54] and indirectly (transformer)[35] coupled to the FCG. Both methods have their advantages and disadvantages. Direct connection seems to work the best. Figure 18 shows the results obtained by Loki for a completely explosive-driven FMG–FCG pulsed-power system. A helical FCG was directly seeded by a single-magnet multiturn FMG. The FMG supplied a seed current of about 300 A to the FCG, which was amplified to 33.5 kA and delivered to a 105-nH load. The current amplification factor was 112. Because the FMG has a very long current pulse (tens of microseconds), it is suitable for seeding FCGs, because the time at which crowbarring takes place is not as critical.

5.2. Power conditioning

The power-conditioning components used with EPP devices are very similar to those used with conventional nonexplosive pulsed-power systems. They include such devices as opening and closing switches, peaking inductors, capacitors, vector inversion generators (VIGs), and so on.

Because FCGs are inherently relatively low-voltage power supplies and many HPM loads require high voltages that are on the order of 400–500 kV, power conditioning is a necessity. An FCG can supply a low impedance load with a high-amplitude current pulse with a rise time on the order of microseconds. Therefore, in order to provide the high voltages and

pulse shapes required by HPM sources, a power-conditioning circuit, which could consist of inductive energy stores and opening switches, must be specially designed to match the FCG with the load.

The University of Missouri–Columbia (UMC) has developed both pulse transformers [Fig. 19(a)] and electroexplosive opening switches (EEOS) [Fig. 19(b)] to provide power conditioning of the FCG output.[29] Additionally, a compact high-power radio frequency (RF) source was developed as a load. The full system is shown in Fig. 20(a). The system inductively stores energy in the pulse transformer, L_{pri} and L_{sec}, during FCG operation. At the end of FCG operation, the rapid rise in the resistance of the EEOS, R_{fuse}, causes energy to be transferred to the secondary circuit, charging the load capacitor C_s to high voltage. The low-inductance switch S_G is designed to self-break at a predetermined high voltage. The load capacitor and the shunt inductor L_{shunt} form a high-frequency oscillator circuit. A high-power antenna in parallel with the capacitor can radiate the RF energy. A resistive load, Z_L, can be substituted for the antenna for nonradiating experiments. All of the power-conditioning and load components were designed and built to fit within a cylindrical housing with a diameter of 15 cm.

Because explosive shots tend to be costly and time consuming, UMC also built an FCG simulator [Fig. 20(b)], which was modeled after a previously developed simulator at TTU,[8] to test their power-conditioning system and RF source. The FCG simulator consists of a high-voltage capacitor bank that discharges into a network of parallel inductors connected by saturating magnetic switches. The inductors L1–L4 have successively smaller inductances to simulate the decreasing inductance of the FCG (Fig. 20). Each magnetic switch saturates and sequentially switches the parallel inductors into the circuit. The FCG simulator at UMC was used to drive a power-conditioning system at full power and an RF source. Peak currents of 20–50 kA with rise times of 8–12 μs were produced.

The pulse transformer developed at UMC performs multiple functions in their compact power-conditioning system. First, it serves as an inductive energy storage element, which stores the energy input from the FCG in the magnetic field of its primary winding during FCG operation. Second, it serves to step up the voltage delivered to the load, while limiting the voltage across the EEOS.

The UMC transformer is based on spiral-strip geometry and has an air core. The windings were made from tapered copper foils and Mylar insulating sheets. The outer diameter of the transformer was 15 cm, and its length was ~18 cm. Because the power-conditioning system was designed to be used with FCGs, it was designed to operate with μH loads. The inductance of the transformer's primary was selected to be 1 μH. The turns ratio was three, and the coupling factor of the transformer was as high as 0.85.

At the end of FCG operation, an opening switch in series with the inductive energy store must open to transfer energy to the load. The electroexplosive switch is a single-shot device that exhibits a dramatic increase in resistance when the metal comprising the conductive path vaporizes due to energy dissipation. Owing to the fast rise in resistance, it was shown that the switch can repeatedly transfer energy to the load in less than 200 ns. The UMC EEOS consisted of a two-section array of parallel silver-plated copper wires. The wires were angled in each of the two sections of the fuse, and copper field shapers provided the form on which the wires were angled. The entire assembly was embedded in a quenching material made of fine glass beads. The EEOS can fail, resulting in a dramatic impedance drop, if an excessively high voltage is across the EEOS. A common cause of this overvoltage condition is stray inductance in the system or incomplete FCG operation at the time of EEOS resistance rise. UMC added a crowbar switch in parallel with the pulse transformer

(a)

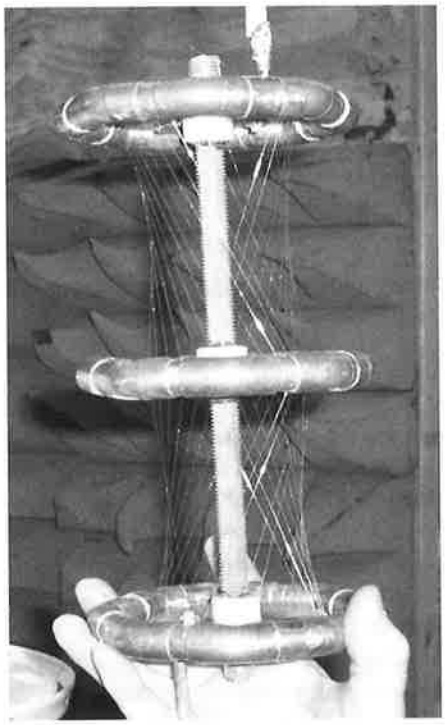

(b)

Fig. 19. (a) Air core transformer and (b) EEOS used in the power-conditioning circuit of an FCG.

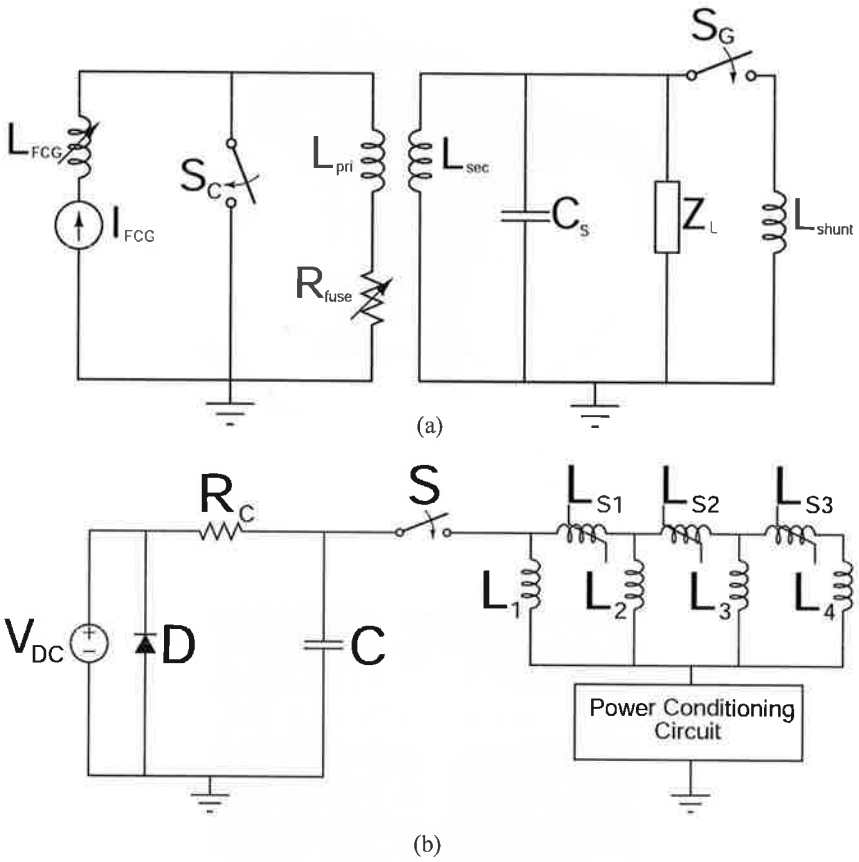

Fig. 20. (a) Schematic of UMC full power-conditioning system and RF load. (b) Schematic of UMC FCG simulator.

and EEOS to limit the effects of stray inductance and to eliminate EEOS restrike during testing.

A high-power RF source was developed as an alternative system load. The RF source consisted of a high-voltage capacitor and a low-inductance oscillating circuit with either a parallel resistive load or a radiating antenna. Triplate, spiral-strip, and coaxial-cylinder geometries with diameters less than 15 cm were tested.[28]

A number of experiments were conducted using the FCG simulator to optimize the performance of the power-conditioning components and RF source. In these experiments, a resistive load was placed in parallel with the RF source circuit to approximate the impedance of free space. After the compact high-voltage capacitor was charged by the power-conditioning system to a peak voltage of approximately 200 kV, the oscillating circuit produces high-power RF pulses with power levels greater than 130 MW and frequency content ranging up to 250 MHz (Fig. 21).[28,29] A series of tests were also conducted at TTU by UMC using TTU's FCGs as the current source. In these experiments, they demonstrated that the power-conditioning system could generate voltages greater than 130 kV across a resistive load, corresponding to a peak RF power of 120 MW (Ref. 39). Experiments conducted using TTU's FCGs and a radiating dipole antenna in place of the resistive load resulted in a peak load voltage greater than 700 kV and peak-to-peak radiated fields of

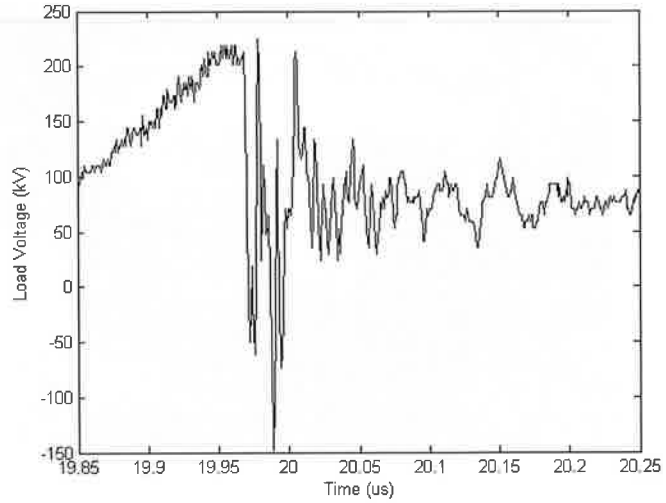

(a)

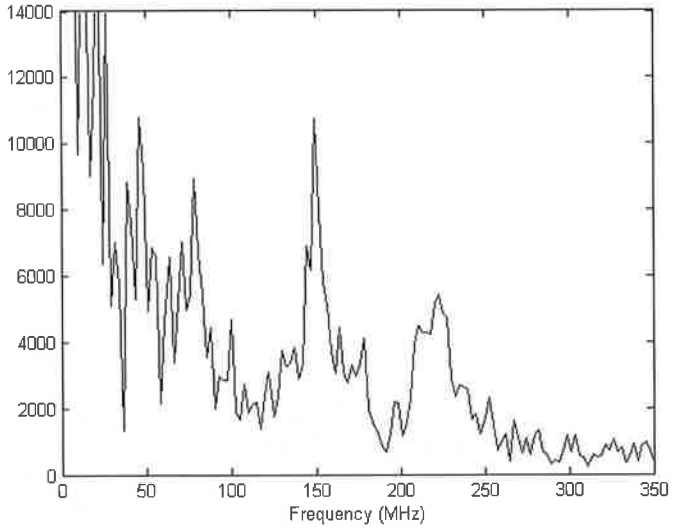

(b)

Fig. 21. (a) Load voltage RF signal produced by power-conditioning system and high-power RF source. (b) Frequency content of high-voltage RF signal.

6 kV/m measured at 5.5 m from the source.[19] Subsequent tests using the UMC FCG simulator with a resistive load in parallel with the oscillating circuit have produced RF powers greater than 250 MW. Work continues to further increase the voltage delivered to the load.

Recent work at UMC on numerical modeling of the power-conditioning system and, specifically, the EEOS has provided new insights into component optimization and design improvements. The results of this modeling work provided an improved method for examining the effects of component changes on system operation and a reexamination of the design processes for electroexplosive opening switches.[27]

(a)

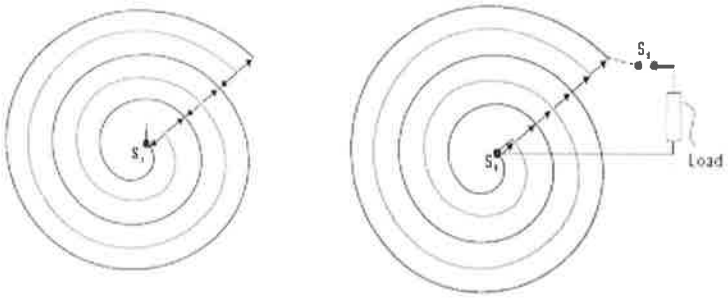

(b)

Fig. 22. (a) Photograph of a VIG in oil and (b) diagrams that explain VIG operation. The lines are the conductors (both red and blue). The space between the lines is the dielectric. The intermediate spaces are insulators. The figure on the left shows the VIG dc charged, and the figure on the right shows it fully erected. The typical energy density is about 30 mJ/cm^3, when operated in a single-shot (destructive) mode and less for repetitive operation.

Another power-conditioning device that looks promising is the VIG (Fig. 22), which was developed by Radiance Technologies. Loki used the VIG as the power-conditioning unit for both their FEGs and FMGs. In one series of experiments, they used a high-voltage FMG to drive a VIG.[41] They found that the VIG increased the voltage output of the FMG by some multiplicative factor (in one shot by a factor of four) that depended on the characteristics of the VIG. They also found that the VIG simultaneously compressed the pulse length from microseconds to a few nanoseconds. In another series of experiments, Loki used a FEG to drive a VIG.[40] In one experiment, the VIG increased the output voltage of the FEG from 11 to 94 kV (Fig. 23). The VIG is a lightweight, compact, versatile power-conditioning device that can be modified to fit many form factors. An energy density of 10 mJ/cm^3 has been achieved with a single-shot VIG.[51]

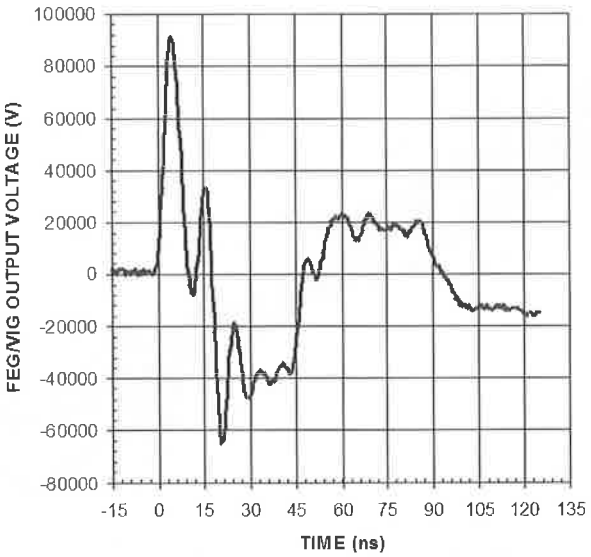

Fig. 23. Explosive-driven FEG–VIG test results: FEG, 6 kV and VIG, 88 kV.

6. Explosive-Driven HPM Test Bed

TTU is developing a compact, explosive-driven HPM test bed. The major design constraints[18,59] were that the system had to do the following:

- Be completely self-contained, i.e., have no external power source.
- Fit into a volume with a diameter no greater than 15 cm and a length no greater than 1.5 m.
- Radiate energy.

The primary objectives of this effort were to develop and optimize the various components of the system, study the issues associated with system integration, and train students in EPP, high-voltage engineering, and HPM.

The major components of the test bed are shown in Fig. 24. As can be seen, it consists of a prime power or seed source for the FCG, a helical FCG, a power-conditioning module, a microwave source, and an antenna. Because the focus of this paper is EPP, attention will be focused only on the fire set, seed source, FCG, and power-conditioning module.

6.1. Fire set

TTU is developing a fire set for the exploding bridgewire (EBW) detonators they use in their FCGs. It consists of a single 1-μF capacitor, a high-voltage dc–dc converter, a battery, and a circuit board. A single NPN BJT transistor is used as a closing switch in a common emitter configuration. Work is underway to reduce its size and to incorporate it into the stand-alone compact seed source (CSS).

6.2. CSS

The CSS (Fig. 25) consists of a 12-V lead-acid battery, a charge limiter circuit, a solid-state high-voltage switching circuit, four step-up dc–dc converters, and a single energy

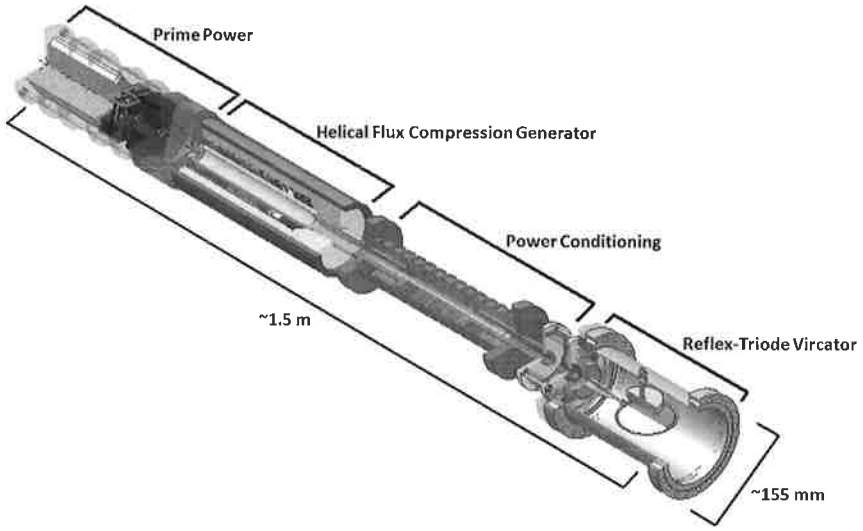

Fig. 24. Explosive-driven HPM test bed.

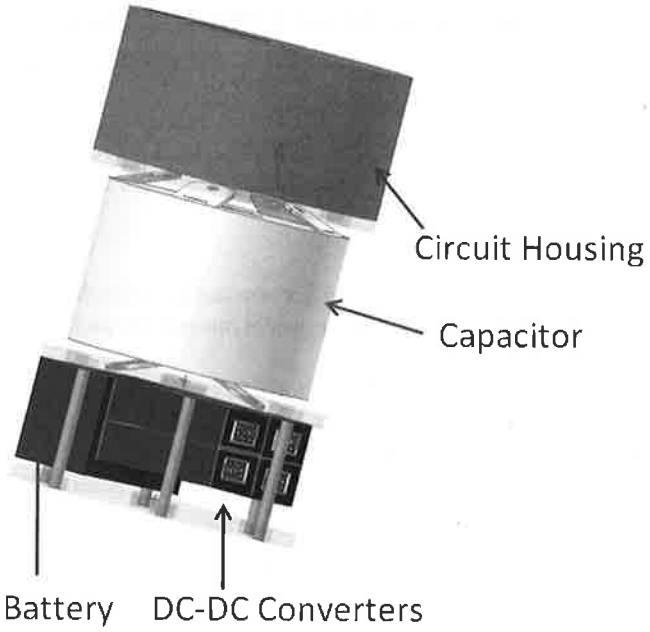

Fig. 25. CSS for FCG: diameter 6 in., height 12 in., weight 8.6 lb, volume 340 in.^{3}, and energy density roughly 100 mJ/cm^3.

storage capacitor. The seed source has a volume of 0.005 m^3 (diameter less than 6 in. and length of 12 in.) and a weight of 3.9 kg (8.6 lb). This source is capable of delivering 360 J and 10 kA to a 6-μH load. The charge time of the seed source is <30 s. A newly designed switching scheme for the seed source uses off-the-shelf high-voltage semiconductor components that minimize system cost and, more important, size.[10] The system energy density

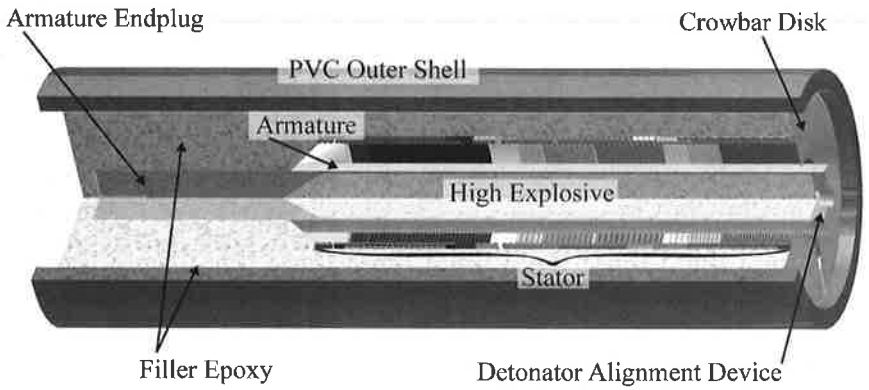

Fig. 26. TTU two-stage FCG. It delivers an electrical energy density of roughly 1 J/cm^3 to a 2.5-μH load.

of the autonomous seed source is 60 mJ/cm^3 to take into account any possible losses in the connections between the seed source and the FCG. Efforts are underway to significantly reduce the charging time of the CSS to less than 1 s, to replace the lead-acid battery with a state-of-the-art Li-ion battery, and to reduce the overall size of the CSS.

6.3. FCG

The TTU helical FCG (Fig. 26) consists of two stages and uses *flux trapping* (also called a *dynamic transformer*) between each stage.[12] The first stage, referred to as the *booster stage*, is coupled to the prime power (seed) source through the first dynamic transformer. The booster stage is responsible for energy gain. The load for the first stage is the primary of the second dynamic transformer in the second stage. The coil of the secondary cascade serves as the secondary of this second transformer. The function of the secondary booster is as a *peaking stage*; i.e., it serves to shorten the length of the current pulse and to increase the output impedance and voltage of the generator.

The overall diameter of the FCG is ~150 mm, and it total length is ~430 mm. The stator and armatures have inner diameters of 76 and 38 mm, respectively. Thus, the expansion ratio of the armature is 2:1.

The armature is a seamless annealed aluminum pipe with a wall thickness of 2.135 mm and a length of 305 mm. The explosive charge is C-4 and has a weight of 410 g. It is connected to a 38-mm-diameter aluminum end plug, which connects the armature to the load and which holds the armature concentric in the generator volume.

The stator has a total length of 254 mm. The booster stage has a length of ~172 mm and is composed of six different sections. Each section is composed of wires having different conductor cross-sectional areas and pitches with a decreasing number of turns of stranded Teflon-insulated, silver-coated copper wire in each succeeding section. The conductor cross-sectional area and pitch is increased in each successive section to compensate for the increasing current density. The wires are also *bifurcated* (paralleling wires in a section to increase the cross-sectional area) in the last three sections, again, to handle the higher current density.

The peaking stage consisted of only two sections. The objective of this stage is to step down the magnitude of the current generated in the booster stage. This has the effect of

shortening the length of the current pulse and increasing the output impedance and voltage of the generator.

The windings in the peaking stage are insulated with Teflon. The primary of the first dynamic transformer is magnet wire with a thin coating of polyamide insulation. This insulation is adequate because the booster stage seed coil voltages do not reach voltage breakdown levels between turns. This dynamic transformer is an air core unit, which means that it has a significantly lower coupling coefficient than magnetic core transformers. The second-stage seed coil is insulated with PVC jacketing to hold off the high voltages that develop between this seed coil and the second stage before the second stage has crowbarred and that develop during second-stage operation.

To switch the booster stage into the circuit and to trap the flux to be compressed, a copper disk, called a *crowbar*, is used. The crowbar should be designed so that the generator volume is closed before there is any appreciable loss of flux. Most FCGs have a glide plane for the armature as it expands outward so that contact with the disk is never lost and the current conduction is continuous. Previous research at TTU showed that the crowbar disk performed, at significantly reduced fabrication cost, as well as the glide planes used in medium-sized generators.[20] A radial cut through one edge of the disk is introduced to prevent eddy currents. In addition, a thin insulator is placed on the edge of the crowbar disk closest to the armature to prevent premature electrical breakdown between the armature and the crowbar disk. Initially, the crowbar for the peaking stage of the FCG was a Teflon-coated pin, but it was removed, and crowbarring is accomplished by the expansion of the armature onto the windings of this stage.

The system energy density of the FCG fired into an inductive (a few microhenrys) load ranges from 300 mJ/cm^3 up to 1 J/cm^3. This number is cut approximately in half if the seed source is included in the equation. Hence, a system consisting of a seed source and an FCG has a *system* or *demonstrated energy density* of several hundred millijoules per cubic centimeter.

6.4. Power conditioning

The power-conditioning system consists of an inductive energy store (IES), peaking gap, and electroexplosive opening switch.[60] The IES (Fig. 27) is simply an intermediate storage device that accumulates the output energy from the FCG and transfers it to the HPM source. The limiting design factor for the IES was its cross-sectional area. Because the FCG delivers tens of kiloamperes, the conductor cross-sectional area must be sufficiently large to minimize resistance, while meeting the diameter constraints of the system. The IES is made by winding PVC-insulated copper wires in parallel onto a cylindrical mandrel with a diameter of 76 mm and coating it with a thick layer of epoxy to keep the turn spacing fixed and to provide insulation between the windings.

The EEOS utilizes several strands of small-diameter ($\sim$100 μm) gold or silver wires that are driven into vaporization on a nanosecond timescale. Because the overall diameter of the system could not exceed $\sim$15 cm, the EEOS (Fig. 27) was placed inside the IES. Metal gears are used to space the wires equidistant from each other. Field-shaping rings are used to suppress fuse restrike by distributing the fields more homogeneously across the gear surface. The switch is charged with SF_6 to quench restrikes. Both the IES and EEOS are placed inside a stainless-steel housing.

The EEOS can be treated as a variable resistor with low initial impedance that increases to very high impedance in a short period of time. The 10-μs rise time of the current pulse from the FCG causes the fuse to operate in two stages. Before the fuse reaches its *action*

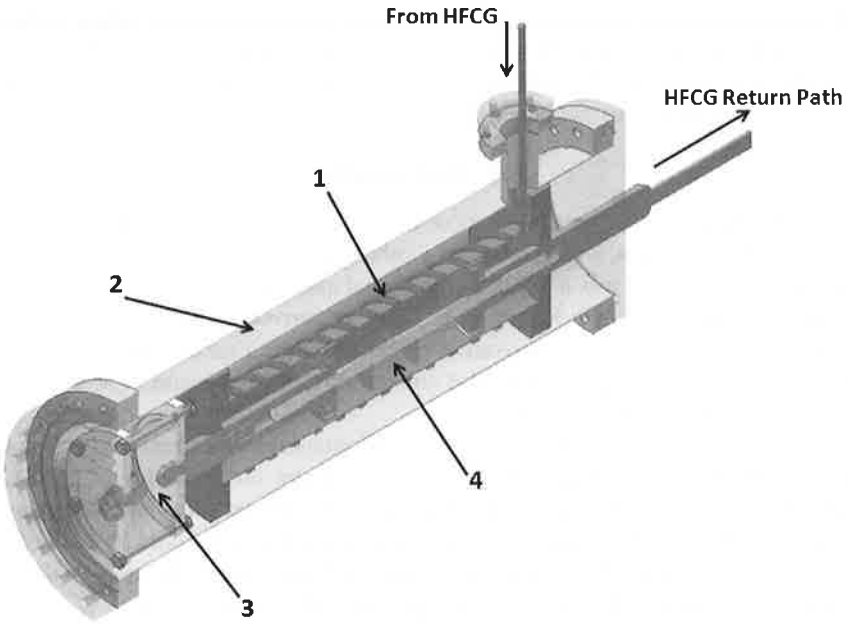

(a)

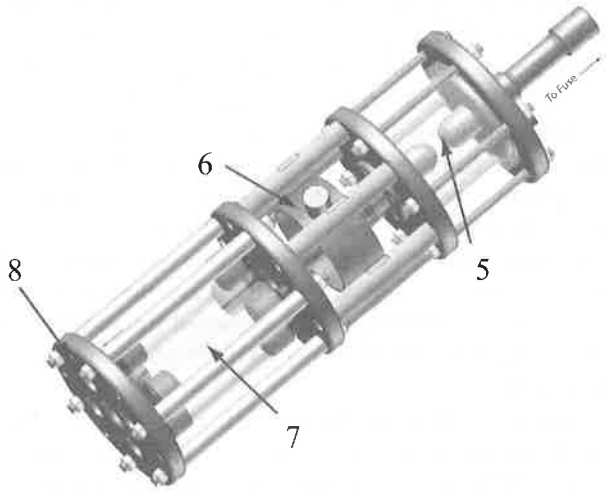

(b)

Fig. 27. TTU (a) IES and (b) EEOS: 1, IES; 2, connection to peaking gap; 3, fuse wire (gold); 4, fuse gear and field shaper; 5, peaking gap; 6, capacitive voltage divider; 7, four parallel 80-Ω water resistors; and 8, ground plate.

limit, the current flowing through the fuse and the finite resistance of the fuse generate a voltage in accordance with Ohm's law. This voltage increases slowly and somewhat linearly as the current increases until the action limit of the switch is reached. As the action limit is approached, the fusing process (vaporization of the wires) begins to take place and the impedance increases rapidly. To prevent plasma formation on the surface of the cathode of

the HPM source and premature closure of the anode–cathode gap, a *peaking gap* [Fig. 27(b), item 5] is introduced between the power-conditioning system and the HPM source. The peaking gap is a simple self-breakdown spark gap that closes on overvoltage. The peaking gap switch was designed to operate in SF_6.

6.5. Test results

To test this EPP system, two loads were used. The first was a resistive dummy load filled with $CuSO_4$ solution, which provides a robust resistance that stays constant even at high currents. The second was a reflex triode virtual cathode oscillator, with time-varying impedance that depends on the history of the driving current. The diagnostics included a Rogowski coil that measures the derivative of the current, a Pearson current monitor that measures the current directly, a capacitive voltage divider to measure high voltages, and antennas to measure radiated microwaves.

The TTU helical FCG has delivered tens of kiloamperes of current and kilojoules of energy to a microhenry inductive load in times that are on the order of 10 μs. This generator typically has energy gains of 14–20, and on multiple shots it has demonstrated energy gains in the 40s. Note that a current gain of more than 200 could be easily reached into a 100-nH inductance, which, however, would spoil the overall efficiency of the system as the power conditioning would suffer greatly from such a small inductance.

TTU demonstrated that the power-conditioning circuit they utilized can transform a slow-rising, high-current output pulse from their helical FCG into a fast-rising, high-voltage pulse that is delivered to their load. They have delivered power and energy levels as high as 1.26 GW and 272 J, respectively, to their resistive load. The action of the fuse after vaporization limited the amount of power delivered to the load. However, by adjusting the parameters of the fuse, it is expected that voltages of 200–300 kV can be delivered by helical FCGs generating currents of 40–45 kA to a few-microhenrys energy storage inductor. A representative system output waveform into a 20-Ohm dummy load is shown in Fig. 28.

Experiments were conducted in which the seed source, FCG, and power-conditioning circuit with a peaking gap were used to drive a Vircator.[25] To date, the maximum radiated power achieved with their FCG-driven Vircator is only about 30 MW with a pulse length of ~150 ns at a frequency of about 4 GHz. It is believed that through further research and engineering this performance can be improved significantly. That is, the Vircator has already shown output powers in excess of 100 MW when driven by a previously developed[8] nonexplosive test bed.

All the objectives of this specific program were met; i.e., they met the form factor requirements, demonstrated radiated microwaves, and trained students in EPP, high-voltage engineering, and HPM. The creation of this explosive-driven test bed will enable their students and researchers alike to conduct plug-and-play experiments.

7. Experimental Observation of RF Radiation Generated by an FEG-Driven Antenna

In 2005, Rader et al.[30] reported on a series of tests conducted by Loki, Inc., in which they used an FEG to drive a dipole antenna through a simple-pulse-forming network. They conducted three test shots using the same dipole antenna and pulse-forming network and FEGs that had identical or similar physical configurations. A receiving dipole antenna, which was similar to the transmitting antenna, was placed approximately 3 m from the

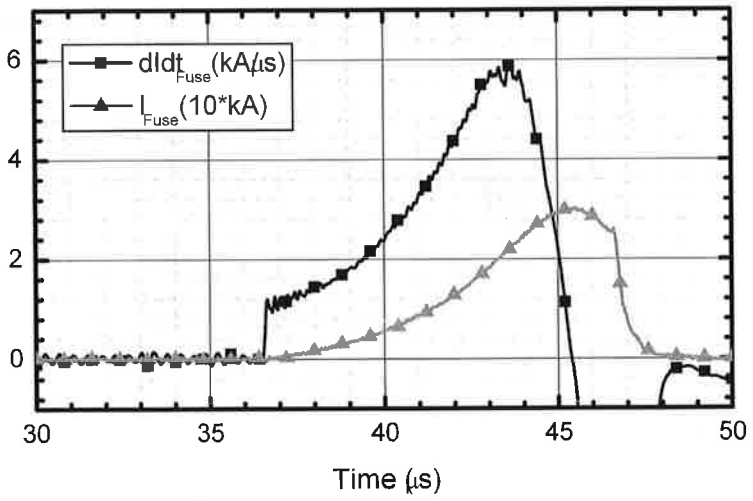

(a)

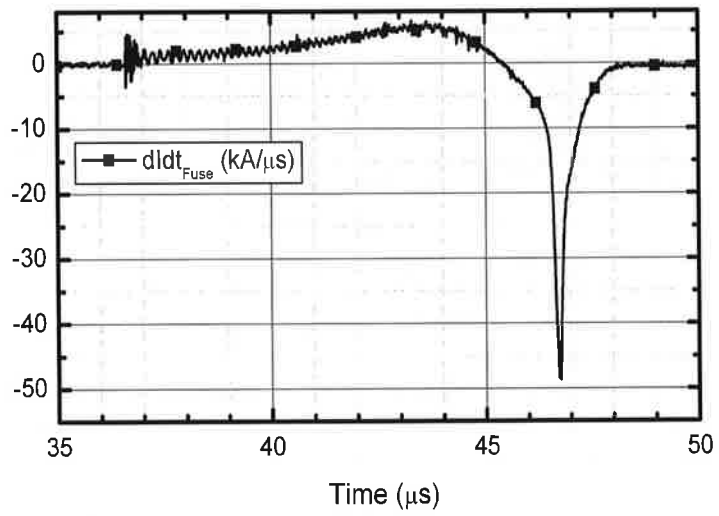

(b)

Fig. 28. (a) FCG output d*I*/d*t* and current waveforms with fuse opening switch and (b) power-conditioned d*I*/d*t* (Ref. 1).

transmitting antenna. The received waveforms were recorded along with the voltage pulse (Fig. 29) delivered by the FEG to the pulse-forming network.

The FEG contained a 2 × ½ × ½ EC-64 PZT element. The FEG used 25 g of RDX high explosive. This generator produces a peak voltage ranging up to 40 kV into an open circuit. The pulse-forming network was constructed using approximately 280 mm of RG-58 coaxial cable. The cable length may be used to control the frequency spectrum of the output

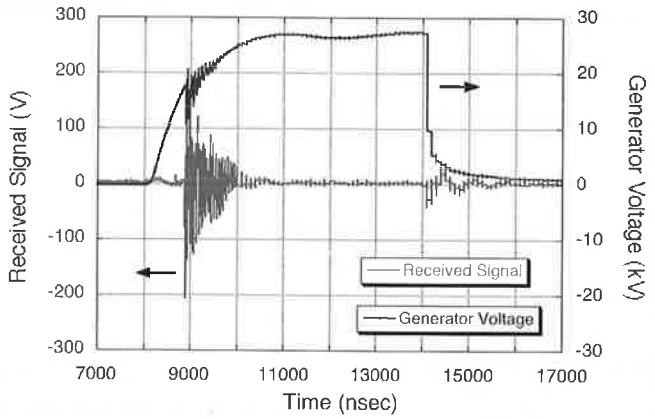

Fig. 29. Voltage generated by FEG and signal received by antenna at 3 m.

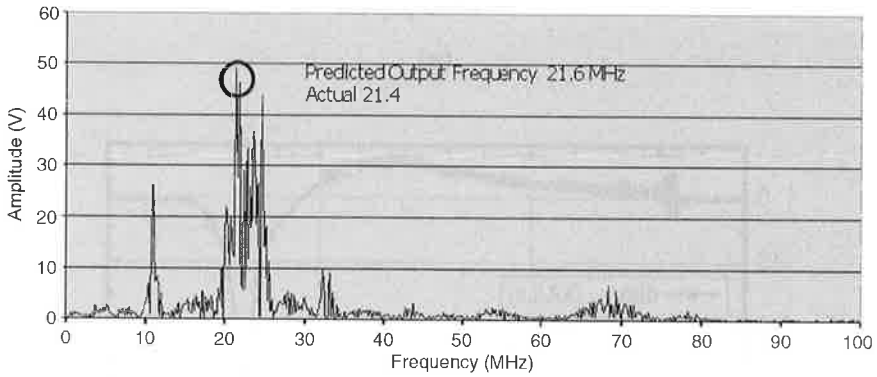

Fig. 30. FFT of the received signal at 3 m.

signal. Because the cable was a 1/4 wavelength impedance-matching circuit, the expected radiated frequency was 21.67 MHz.

A spark gap was placed between the inner conductor of the coaxial cable and the antenna. The antenna was V-shaped, and each leg had a length of 1 m. The resonant frequency of the antenna was estimated to be about 75 MHz. The receiving antenna was similarly constructed.

Each shot produced what appeared to be two RF bursts that coincided with rapid changes in the source voltage. The first RF burst produced a pulse with a peak voltage amplitude of -30 V peak to peak and lasted for 1 μs. The second burst produced a pulse with voltage amplitude of 50 V peak to peak that also lasted for 1 μs. The true peak voltage of the second burst could not be determined because the second burst saturated the input of the oscilloscope.

Using the peak voltages picked up by the receive antenna, the peak power density at the antenna was calculated to be 1.64 W/cm^2 and the effective radiated power (ERP) at the source antenna was calculated to be 2 MW, assuming that the receiving antenna had a gain near unity. The FEG generated about 2.4 MW of electrical power.

A fast Fourier transform (FFT) (Fig. 30) revealed that the spectrum of the RF bursts was concentrated between 18 and 26 MHz, with the largest signal at 21.4 MHz, which is in good agreement with the predicted value of 21.67 MHz.

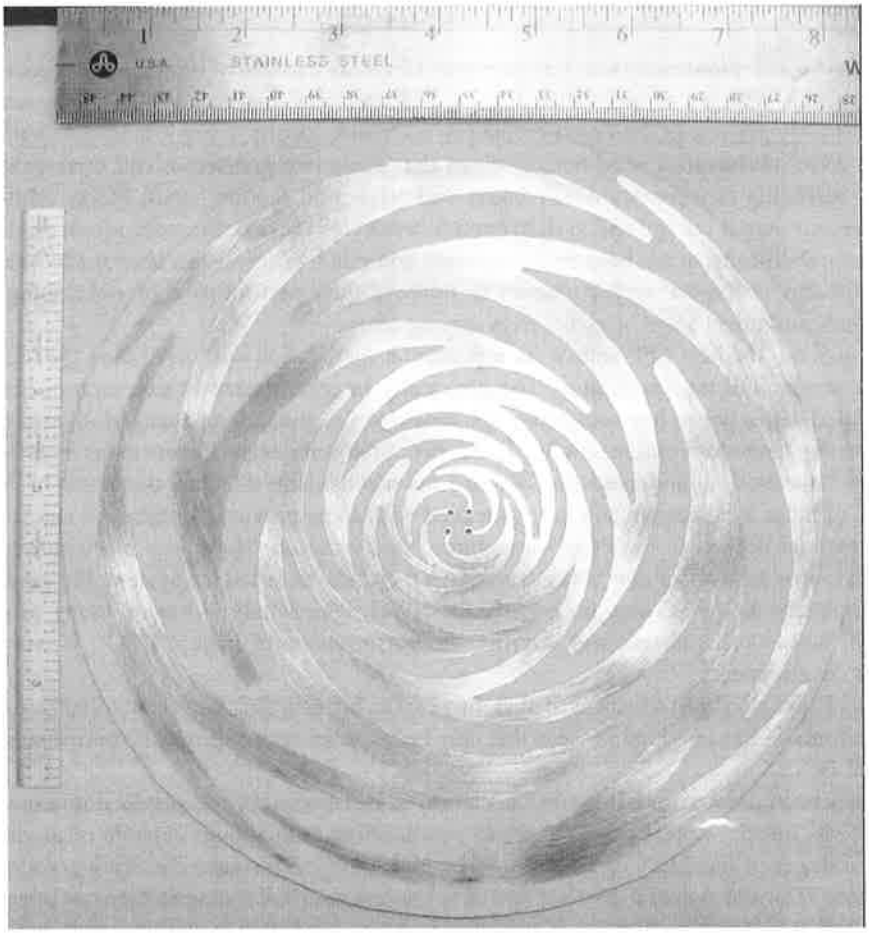

Fig. 31. Sinuous antenna.[52]

Utilizing two independent field diagnostic techniques, it was demonstrated that a similar FEG-dipole antenna setup radiated a frequency of around 100 MHz (Ref. 30). One field probe was an electric field sensor transmitting back into the diagnostics screen room over a fiber-optic cable, and the other sensor was a D-dot probe matched with a wideband balun. Both probes recorded a maximum peak-to-peak electric field of around 850 V/m at a range of 5 m, giving a field-range product of about 4.2 kV.

Subsequently, tests were also successfully performed by Stults[52] and by TTU and UMC. The latter tests were described in Sec. 5.2. Unlike Rader and TTU/UMC, which used dipole antennas, Stults drove a sinuous antenna (Fig. 31). Sinuous antennas have several advantages over other antennas when impulse loaded. They are frequency-independent and circularly polarized and can be driven by significant voltages without electrical breakdown. Stults successfully demonstrated that FEGs are suitable for driving such antennas. He reported on the first multipulse system, which consisted of a single FEG and a sinuous antenna. This system radiated 13 pulses at a frequency of 100 MHz and a repetition rate of 2.3 MHz.

8. Conclusions

It has been demonstrated that very compact FEGs are capable of reproducibly generating open-circuit voltages of more than 100 kV and that very compact FMGs are capable of reproducibly generating tens of kiloamperes, both with specific energy densities approaching 1 J/cm^3. It has also been demonstrated that these two generators can drive practical loads including charging capacitor banks and VIGs and seeding small FCGs. Although the present output energy and system energy density of these devices are relatively small, their capabilities have not been fully exploited and much progress has been made just over the past few years. So work continues to improve their performance by developing new materials and novel ways of explosively driving them.

In general, the best EPP source for a particular application will depend on the load, its environment, and the application. The physically larger, midsize FCGs, such as the one presented in this paper, have output energy densities, i.e., the ratio of energy delivered to the load to the generator volume, is a few joules per cubic centimeter. Recent experiments have further improved our understanding of those loss mechanisms that limit the output of FCGs. Some of these loss mechanisms are associated with some previously unknown mechanical and material defects in the FCG's armatures. Understanding these loss mechanisms will now allow us to look for new ways to engineer these losses out of the system. For example, a completely new FCG design, namely the SWG, which may eliminate many of these known failure mechanisms and improve the performance of helical FCGs, is currently under development.

There have also been advances in modeling FCGs. In particular, the recent resistance point contact model has provided insights that may help researchers improve the performance of helical FCGs.

It has been demonstrated that FCGs can drive HPM sources and produce microwaves. The UMC has developed compact power-conditioning components capable of producing load voltages of hundreds of kilovolts and a high-power RF source for driving wideband antennas. The addition of a crowbar switch to the power-conditioning system has improved the reliability of compact opening switches, and new modeling techniques have provided advanced design capabilities. It has also been shown that FEGs can direct drive antennas and produce radiated RF.

Finally, TTU created a test bed that incorporates all the major components of a self-contained explosive-driven HPM system. This will enable them and other researchers to test new components, address integrations issues, and train students in EPP, high-voltage engineering, and HPM.

References

[1]Altgilbers, L.L., "Explosive Pulsed Power: An Enabling Technology," 26th Army Science Conference, Orlando, FL, December 2008.

[2]Altgilbers, L.L., M.D.J. Brown, I. Grishnaev, B.M. Nova, I.R. Smith, I. Tkach, and Y. Tkach, *Magnetocumulative Generators*, Springer-Verlag, New York (2000).

[3]Baird, J., and S.I. Shkuratov, "Ferroelectric Energy Generator, System, and Method." Patent pending, Application No. 11/461,349. Filing date 7/31/2006.

[4]Baird, J., S.I. Shkuratov, and E.F. Talantsev, "Ferromagnetic Energy Generator, System, and Method." Patent pending. Filing date 7/31/2006.

[5]Baird, J., and P.N. Worsey, Digest of Technical Papers, 2001 IEEE Pulsed Power and Plasma Science **1,** 94 (2001).

[6]Baird, J., P.N. Worsey, and M. Schmidt, Digest of Technical Papers, 2001 IEEE Pulsed Power and Plasma Science **2**, 953 (2001).

[7]Barmin, A.A., and A.B. Prishchepenko, "Compression of a Magnetic Field in a Single Crystal by a Strong Converging Ionizing Shock Wave," in *Megagauss Magnetic Field Generation and Pulsed Power Applications*, Part 1 (edited by M. Cowan and R.B. Spielman), Nova Science Publishers, Inc., Commack, NY, pp. 35–40 (1994).

[8]Belt, D., J. Mankowski, A. Neuber, J. Dickens, and M. Kristiansen, Rev. Sci. Instrum. **77**, 094702 (2006).

[9]Bichenkov, E.I., "Shock Wave Driven Flux Compression Technique," in *Megagauss Magnetic Field Generation, Its Application to Science and Ultra-High Pulsed Power Technology* (edited by H.J. Schneider-Muntau), World Scientific, Singapore, pp. 593–598 (2004).

[10]Elsayed, M., T. Holt, A. Young, A. Neuber, J. Dickens, M. Kristiansen, L.L. Altgilbers, and A.H. Stults, "High-Current Compact FCG Seed Source Implementing Solid State Switching," in *Proceedings of the 2008 IEEE International Power Modulator Conference*, Las Vegas, NV, May 27–31, 2008 (to be published).

[11]Freeman, B.L., private communications, June 2008.

[12]Freeman, B.L., and A.A. Neuber, "Loss Mechanism Basics," in *Explosively Driven Pulsed Power, Helical Magnetic Flux Compression Generators* (edited by A. Neuber), Springer Verlag (2005).

[13]Gilev, S.D., Combustion Explosion Shock Waves **41**, 599 (2005).

[14]Gilev, S.D., "Shock Wave Cumulation of Magnetic Field: Building Physical Model of the Phenomenon," in *Proceedings of Megagauss XI*, London, September 2006 (to be published).

[15]Hemmert, D., J. Dickens, J. Mankowski, J. Walter, S. Holt, and M. Kristiansen, "Shock Induced Conductivity of Aluminum Powder for Closing Switches for Ultracompact Explosive Generators," in *Proceedings of 14th International Symposium on High Current Electronics*, Tomsk, Russia, pp. 290–293 (2006).

[16]Hemmert, D., S. Holt, and J. Krile, "Electrical Breakdown of Aluminum Powder in Shock Wave Driven Pulsed Power Systems," Directed Energy Professional Society, 10th Annual Directed Energy Symposium, Huntsville, AL, November 5–8, 2007.

[17]Holt, S.L., D.J. Hemmert, J.T. Krile, W.S. Hackenberger, E.F. Alberta, J.W. Walker, J.C. Dickens, L.L. Altgilbers, and A.H. Stults, "Testing of New Ferroelectric Materials for Explosively Driven Ferroelectric Generators," in *Megagauss XI*, London, 2006 (to be published).

[18]Holt, T.A., "Design of a Dual-Stage Helical Flux Compression Generator," Ph.D. Dissertation, Texas Tech University (2008).

[19]Holt, T.A., A.J. Young, M.A. Elsayed, A.A. Neuber, M. Kristiansen, K.A. O'Connor, and R.D. Curry, "Investigation of an FCG and Pulse Transformer Based Power Conditioning System," in *Proceedings of the 2007 IEEE Pulsed Power and Plasma Science Conference*, Albuquerque, NM, June 17–22, 2007.

[20]Holt, T.A., A.J. Young, A.A. Neuber, and M. Kristiansen, "A Fabrication Method for a Mid-Sized, High Energy-Density, Flux Compression Generator," in *Proceedings of the 2006 International Conference on Megagauss Magnetic Field Generation and Related Topics*, Santa Fe, NM, Omnipress, pp. 281–286 (2008).

[21]Kiuttu, G.F., and J.B. Chase, "An Armature-Stator Contact Resistance Model for Explosively Driven Helical Magnetic Flux Compression Generators," in *2005 IEEE Pulsed Power Conference*, pp. 435–440 (2005); G.F. Kiuttu, J.B. Chase, D.M. Chato, and F.D. Peterson, "Recent Advances in Modeling Helical FCGs," in *Proceedings of Megagauss XI*, Santa Fe, NM, Omnipress, pp. 255–264 (2006).

[22]Kolosenok, S.V., V.S. Soukhomlinov, Y.A. Tolmachev, and L.L. Altgilbers, Electromagnetic Phenomena **7**(2(19)), 170 (2007).

[23]Kulterman, R.W., G.W. Anderson, and F.W. Neilson, J. Appl. Phys. **29**, 500 (1958).

[24]Neilson, F.W., Bull. Am. Phys. Soc. **2**, 302 (1957).

[25]Neuber, A.A., A.J. Young, J.W. Walter, M.A. Elsayed, T.A. Holt, and M. Kristiansen, "Comparison of HFCG and Compact Marx for Driving a High Power Load," in *Proceedings of the Megagauss XII Conference*, Novosibirsk, Russia, July 12–18, 2008 (to be published).

[26]Novac, B.M., I.R. Smith, and S.E. Goh, J. Phys. D: Appl. Phys. **34**, 174 (2001).

[27]O'Connor, K.A., "Investigation of a High Voltage, High Frequency Power Conditioning System for Use with Flux Compression Generators," Master's Thesis, University of Missouri–Columbia (2008).

[28]O'Connor, K.A., and R.D. Curry, "Experimental Results of a High Voltage Wideband Load Driven by a Pulse Transformer and Opening Switch Power Conditioning System," in *Proceedings of the 2008 IEEE International Power Modulator Conference*, Las Vegas, NV, pp. 185–188 (2008).

[29]O'Connor, K.A., R.D. Curry, and L. Altgilbers, "Investigation of a High Voltage, High Frequency Power Conditioning System for Use with Flux Compression Generators," in *Proceedings of the 2007 IEEE Pulsed Power and Plasma Science Conference*, Albuquerque, NM, June 17–22, 2007.

[30]Rader, M.S., C. Sullivan, and T.D. Andreadis, "Experimental Observation of RF Radiation Generated by an Explosively Driven Voltage Generator," Naval Research Laboratory Rep. NRL/FR/5745-05-10,122 (2005).

[31]Setchell, R.E., J. Appl. Phys. **94**, 573 (2003).

[32]Shkuratov, S.I., M. Kristiansen, J. Dickens, A. Neuber, L.L. Altgilbers, P.T. Tracy, and Y. Tkach, "Experimental Study of Compact Explosive Driven Shock Wave Ferroelectric Generators," Digest of Technical Papers, 13th IEEE International Pulsed Power Conference, pp. 959–962 (2001).

[33]Shkuratov, S.I., E.F. Talantsev, J. Baird, L.L. Altgilbers, and A.H. Stults, Rev. Sci. Instrum. **77**, 066107 (2006).

[34]Shkuratov, S.I., E.F. Talantsev, J. Baird, L.L. Altgilbers, and A.H. Stults. IEEE Trans. Plasma Sci. **34**(5), 1866 (2006).

[35]Shkuratov, S.I., E.F. Talantsev, J. Baird, L.L. Altgilbers, and A.H. Stults, "Transformer-Type Seeding System of a Helical FCG Based on a Transverse Shock Wave Ferromagnetic Generator," in *IEEE Proceedings of 2006 International Conference on Megagauss Magnetic Field Generation and Related Topics* (edited by J.F. Kiuttu, R.E. Reinovsky, and P.J. Turchi), pp. 313–318 (2007).

[36]Shkuratov, S.I., E.F. Talantsev, J. Baird, L.L. Altgilbers, and A.H. Stults, "A New Concept of Explosive Pulsed Power: Design of Macro Primary Power Sources Based on Elementary Miniature Shock-Wave Ferromagnetic Cells," in *IEEE Proceedings of 2006 International Conference on Megagauss Magnetic Field Generation and Related Topics* (edited by J.F. Kiuttu, R.E. Reinovsky, and P.J. Turchi), pp. 319–324 (2007).

[37]Shkuratov, S.I., E.F. Talantsev, J. Baird, L.L. Altgilbers, and A.H. Stults, "New Concept for Constructing an Autonomous Completely Explosive Pulsed Power System: Transverse Shock Wave Ferromagnetic Primary Power Source and Loop Flux Compression Amplifier," in *IEEE Proceedings of 2006 International Conference on Megagauss Magnetic Field Generation and Related Topics* (edited by J.F. Kiuttu, R.E. Reinovsky, and P.J. Turchi), pp. 331–336 (2007).

[38]Shkuratov, S.I., E.F. Talantsev, J. Baird, L.L. Altgilbers, and A.H. Stults, "Compact Autonomous Completely Explosive Pulsed Power System Based on Transverse Shock Wave Demagnetization of $Nd_2Fe_{14}B$ and Magnctic Flux Compression," in *IEEE Proceedings of 2006 International Conference on Megagauss Magnetic Field Generation and Related Topics* (edited by J.F. Kiuttu, R.E. Reinovsky, and P.J. Turchi), pp. 337–342 (2007).

[39]Shkuratov, S.I., E.F. Talantsev, J. Baird, A.V. Ponomarev, L.L. Altgilbers, and A.H. Stults, IEEE Trans. Plasma Sci. **36**(1), 44 (2008).

[40]Shkuratov, S.I., E.F. Talantsev, J. Baird, M.F. Rose, Z. Shotts, L.L. Altgilbers, and A.H. Stults, Rev. Sci. Instrum. **77**, 043904 (2006).

[41]Shkuratov, S.I., E.F. Talantsev, J. Baird, M.F. Rose, Z. Shotts, Z. Roberts, L.L. Altgilbers, and A.H. Stults, IEEE Trans. Plasma Sci. **34**(5), 1866 (2006).

[42]Shkuratov, S.I., E.F. Talantsev, J. Baird, H. Temkin, L.L. Altgilbers, and A.H. Stults, AIP Proc. **845**, 1169 (2006).

[43]Shkuratov, S.I., E.F. Talantsev, J. Baird, H. Temkin, Y. Tkach, L.L. Altgilbers, and A.H. Stults, "Depolarization of a Pb(Zr52Ti48)O3 Polycrystalline Piezoelectric Energy-Carrying Element of Compact Pulsed Power Generator by a Longitudinal Shock Wave," Digest of Technical Papers, 15th International Pulsed Power Conference, pp. 529–532 (2005).

[44]Shkuratov, S.I., E.F. Talantsev, J.C. Dickens, and M. Kristiansen, J. Appl. Phys. **91**, 3007 (2002).

[45]Shkuratov, S.I., E.F. Talantsev, J.C. Dickens, and M. Kristiansen, J. Appl. Phys. **92**, 159 (2002).

[46]Shkuratov, S.I., E.F. Talantsev, J.C. Dickens, and M. Kristiansen, IEEE Trans. Plasma Sci. **30**, 1681 (2002).

[47]Shkuratov, S.I., E.F. Talantsev, J.C. Dickens, and M. Kristiansen, Rev. Sci. Instrum. **73**, 2738 (2002).

[48]Shkuratov, S.I., E.F. Talantsev, J.C. Dickens, and M. Kristiansen, J. Appl. Phys. **93**, 4529 (2003).

[49]Shkuratov, S.I., E.F. Talantsev, J.C. Dickens, M. Kristiansen, and J. Baird, Appl. Phys. Lett. **82**, 1248 (2003).

[50]Shkuratov, S.I., E.F. Talantsev, L. Menon, H. Temkin, J. Baird, and L.L. Altgilbers, Rev. Sci. Instrum. **75**(8), 2766 (2004).

[51]Shotts, Z., Z. Roberts, and M.F. Rose, "Design Principles for Vector Inversion Generators," in *Proceedings of the 2007 IEEE Pulsed Power and Plasma Science Conference*, Albuquerque, NM, pp. 556–559 (2007).

[52]Stults, A.H., "Impulse Loading of Sinuous Antennas by Ferroelectric Generators," in *Proceedings of the 2008 IEEE International Power Modulator Conference*, Las Vegas, NV, May 27–31 (2008).

[53]Talantsev, E.F., S.I. Shkuratov, J. Baird, L.L. Altgilbers, and A.H. Stults, "Analytical Method for Calculation of Currents Produced by Shock Wave Ferromagnetic Generators," Digest of Technical Papers, 16th International Pulsed Power Conference, pp. 1141–1144 (2007).

[54]Talantsev, E.F., S.I. Shkuratov, J.C. Dickens, and M. Kristiansen, Rev. Sci. Instrum. **74**, 225 (2003).

[55]Tkach, Y., S.I. Shkuratov, E.F. Talantsev, M. Kristiansen, J. Dickens, L.L. Altgilbers, and P.T. Tracy, IEEE Trans. Plasma Sci. **30**(5), 1665 (2002).

[56]Tracy, P., L. Altgilbers, I. Merritt, and M. Brown, "Shock Compression of Magnetic Fields in CsI," in *Megagauss Magnetic Field Generation, Its Application of Science and Ultra-high Power Pulsed-Power Technology* (edited by H.J. Schneider-Muntau), World Scientific, Singapore, pp. 450–457 (2004).

[57]Velikovich, A.L., J. Tech. Phys. **62**, 47 (1992) (in Russian).

[58]Worsey, P., J. Baird, and J. Rasty, "Mechanical Aspects of Helical Flux Compression Generators," in *Explosively Driven Pulsed Power, Helical Magnetic Flux Compression Generators* (edited by A. Neuber), Springer Verlag (2005).

[59]Young, A., "Explosively Driven Pulsed Power for High Power Microwave Generation," Master's Thesis, Texas Tech University (2008).

[60]Young, A.J., T.A. Holt, M.A. Elsayed, A.A. Neuber, M. Kristiansen, L.L. Altgilbers, and A.H. Stults, "Fuse and Load Testing with Mid-Sized, High Energy Density Flux Compression Generators," in *Proceedings of the 2007 IEEE Pulsed Power and Plasma Science Conference*, Albuquerque, NM, pp. 1165–1168 (2007).

Technical Scope of Submissions

The Journal of Directed Energy solicits and publishes papers in all aspects of DE, and with particular emphasis on the engineering issues of the discipline, including but not limited to the following:

DE System Design
High Energy Lasers
Laser Optics
Acquisition, Tracking, and Pointing
Propagation Effects
High Power Microwave Sources
Pulsed Electromagnetics
Antenna Systems
Vulnerability Assessment
DE Modeling and Simulation
Human Factors
Self Protection Issues
Test and Evaluation

Instructions for authors:

Manuscripts should be submitted electronically as Microsoft Word or PDF documents to either editor. Include full information (*including address, phone, fax, and e-mail*) for corresponding author to receive proofs. Supply names and contact information of five suggested reviewers, although the editors reserve the right to choose their own reviewers independent of the list supplied. Queries to the author will be typeset in the proof, and proofs will be e-mailed to authors as pdf files, or mailed if e-mail not available. Authors will relay corrections to compositor by e-mail, fax, or mail.

Authors must submit the DEPS copyright form with the paper so that the editor may accept the paper for review, along with written assurance that appropriate security clearance has been obtained. It is the author's responsibility also to provide written assurance that the paper has not been published, nor under consideration, elsewhere and they are willing to make revisions in the paper, if necessary.

Papers should be in American rather than British spelling, using the serial comma, with the use of standard abbreviations for units. (g not gm for gram, for example) Metric or dual systems of units (metric and English) are allowed. Authors should spell out numbers through ten except when used with a unit. Numbers should use the comma in numerals of four or more digits. Papers may use "et al." in the text but the authors need to include all names in the reference list. Acronyms (except for designations) would have to be spelled out at first use and would be allowed even if not used again. Authors should follow standards for setting math given in the book Mathematics in Type.

Papers must include a brief (100 to 200 word) abstract that explains the object of the investigation and the major results. For indexing purposes three to five keywords must be indicated. A nomenclature section must follow the abstract in which all symbols are identified. An introduction explaining previous work and the contribution provided by the submitted paper follows the nomenclature section. A section clearly explaining the conclusions that may be drawn from the results and their significance is the last section of the text, followed by the list of references, tables in numerical order, and then the figures in numerical order. Papers should be no more than 32 double-spaced, 12-point font, pages long in total.

References must be easily accessible public documents and are to be placed at the end of the paper in alphabetical order by first author's last name. References, figures, and tables have to be mentioned in the text. Tables must have a double rule at the top and bottom of the table with a single rule under column headings, with any footnotes placed under the bottom double rule. Illustrations must be clear and sharp with lettering large enough to be easily legible. Each figure must be a separate page and the captions should be listed in numerical order on a separate page. Table and figures can be mentioned out of order parenthetically (that is, a figure that is discussed later could be referred to earlier) Reference callouts in figures or tables are adequate; it's not necessary that the references also be mentioned in the text. Photographs must be glossy prints. Footnotes to the text are acceptable.

Color illustrations or photographs will be published if the editors deem it necessary for clarity. Use of color involves substantial expense and the author's employer must pay the full incremental cost of color publication (minimum of $1000 for production costs, plus $75 per figure for color separations; actual costs may vary).

The JDE will not accept papers for publication that do not adequately address the accuracy of the results, whether computational or experimental.